Neuronal membrane glycoprotein (nmgp-1) gene deficiency affects chemosensation-related behaviors, dauer exit and egg-laying in *Caenorhabditis elegans*

Eliana M. Fernández[1], Yamila B. Cutraro[1], Jessica Adams[2], Melisa C. Monteleone[1], Kiley Hughes[2] Alberto C. Frasch[1], Andrés Vidal-Gadea[2], Marcela A. Brocco[1]

[1]Instituto de Investigaciones Biotecnológicas, Universidad Nacional de San Martín (UNSAM); Consejo Nacional de Investigaciones Científicas y Técnicas (CONICET) San Martín; Buenos Aires, Argentina

[2]School of Biological Sciences, Illinois State University, Normal, IL, USA

Correspondence to Marcela A. Brocco: Email: mbrocco@iib.unsam.edu.ar, marcelabrocco2002@gmail.com

Av 25 de mayo y Francia.

Campus Miguelete. Edificio IIB.

San Martin. Buenos Aires CP 1650.

Argentina

Tel: +54 11 40061500 ext. 2128

FAX: +54 11 40061500 ext. 2143

Eliana M. Fernández: emfernandez@iibintech.com.ar

Yamila B. Cutraro: ycutraro@iibintech.com.ar

Melisa C. Monteleone: mmonteleone@iibintech.com.ar

Alberto C. Frasch: cfrasch@unsam.edu.ar

Running title: *C. elegans* requires *nmgp-1* for stress recovery

This article has been accepted for publication and undergone full peer review but has not been through the copyediting, typesetting, pagination and proofreading process, which may lead to differences between this version and the Version of Record. Please cite this article as doi: 10.1111/JNC.15543

Keywords: stress, nervous system, PLP family, GPM6A, ASJ neurons, bag-of-worms, neuropsychiatric diseases, chemotaxis, gene expression

Abbreviations: GPM6A, neuronal membrane glycoprotein M6a; NMGP-1 neuronal membrane glycoprotein 1

Date of initial submission: March, 2nd 2021.

Date of 1st resubmission: August, 13th 2021

Date of 2nd resubmission: November, 10th 2021

Abstract count: 200

Introduction + Results + Discussion + Legends count: 8673

ABSTRACT

The nervous system monitors the environment to maintain homeostasis, which can be affected by stressful conditions. Using mammalian models of chronic stress, we previously observed altered brain levels of GPM6A, a protein involved in neuronal morphology. However, GPM6A's role in systemic stress responses remains unresolved. The nematode *Caenorhabditis elegans* expresses a GPM6A ortholog, the neuronal membrane glycoprotein 1 (NMGP-1). Because of the shared features between nematode and mammalian nervous systems and the vast genetic tools available in *C. elegans*, we used the worm to elucidate the role of GPM6A in the stress response. We first identified *nmgp-1* expression in different amphid and phasmid neurons. To understand the *nmgp-1* role, we characterized the behavior of *nmgp-1(RNAi)* animals and two *nmgp-1* mutant alleles. Compared to control animals, mutant and RNAi-treated worms exhibited increased recovery time from the stress-resistant dauer stage, altered SDS chemosensation and reduced egg-laying rate resulting in egg retention (bag-of-worms phenotype). Silencing of *nmgp-1* expression induced morphological abnormalities in the ASJ sensory neurons, partly responsible for dauer exit. These results indicate that *nmgp-1* is required for neuronal morphology and for behaviors associated with chemosensation. Finally, we propose *nmgp-1* mutants as a tool to screen drugs for human nervous system pathologies.

INTRODUCTION

Environmental sensation refers to the process of detecting and encoding an organism's milieu. An animal's survival depends on its nervous system's ability to rapidly integrate relevant environmental cues and trigger appropriate adaptive responses. To this end, they use their sensory systems to detect meaningful changes to environmental variables (Hsieh et al. 2017) and produce both metabolic and behavioral responses. An animal's ability to adapt to fluctuating environments is a form of homeostatic plasticity (Pigliucci *et al.* 2006). In humans, these processes maintain the individual within permissible physiological ranges. However, continued exposure to adverse environments (e.g., limited food, predators, abuse, chronic stress, etc.) can challenge homeostatic processes beyond their functional limits. When this occurs, individuals undergo physiological damage. In humans for example, stress can induce several diseases including neuropsychiatric illnesses such as depression or schizophrenia (Nestler et al. 2002).

We study the molecular bases of neural plasticity and its role in stress responses to understand stress related diseases. Our studies in animal models of psychosocial (Alfonso *et al.* 2004), physical (Alfonso *et al.* 2006) and prenatal stress (Monteleone *et al.* 2014) revealed that stress altered brain levels of M6a (GPM6A), a neuronal membrane glycoprotein. Notably, in psychosocial and physical stress models, antidepressant (tianeptine and clomipramine) treatments restore GPM6A mRNA levels to that of the control animals (Alfonso *et al.* 2004; Alfonso *et al.* 2006). In humans, post-mortem analysis from the brains of depression-associated suicides revealed reduced hippocampal GPM6A mRNA levels with respect to non-psychiatric controls (Fuchsova *et al.* 2015). In addition, *GPM6A* gene polymorphisms are associated with pathological conditions such as schizophrenia (Boks *et al.* 2008), bipolar disorders (Greenwood *et al.* 2012) and claustrophobia (El-Kordi *et al.* 2013). In mammals, GPM6A is expressed predominantly in the central nervous system, particularly in hippocampus, cortex, forebrain, cerebellum and retina (Alfonso *et al.* 2005; Yan *et al.* 1996; Lagenaur *et al.* 1992; Zhao *et al.* 2008). We (and others) have shown that GPM6A participates in neurodevelopmental processes, including neuronal differentiation (Mukobata *et al.* 2002; Michibata *et al.* 2008), neurite extension (Formoso *et al.* 2015a; Alfonso *et al.* 2005), filopodium/spine formation and synaptogenesis (Brocco *et al.* 2010; Fuchsova *et al.* 2009; Zhao *et al.* 2008). GPM6A together with M6, the *D. melanogaster* ortholog (Zappia *et al.* 2012; Zappia *et al.* 2011), belong to the proteolipidic protein (PLP) family that includes the mammalian glycoproteins GPM6A, GPM6B, PLP1 and its isoform DM20 (Stecca *et al.* 2000). Based on GPM6A's established cellular functions we hypothesize that it serves as a signal to promote neuronal

plasticity and therefore to counteract the deleterious effects of stress. However, the involvement of GPM6A in the stress responses remains unclear.

We used the nematode model *Caenorhabditis elegans* to elucidate the role of GPM6A in stress responses. *C. elegans* has near 50 % homology with humans (Kim *et al.* 2018, Lai *et al.* 2000). It has a sensory system that detects the environment and controls physiology and behaviors to maintain homeostasis. Because of the stereotyped behaviors and the available tools to study and manipulate this organism, *C. elegans* is a useful model to dissect the molecules and mechanisms underlying normal sensory system function (Iliff and Xu 2020). Moreover, the worm connectome is fully mapped (White, 1986). Abnormal processing and integration of sensory information is the hallmark of several neurological diseases, including autism, schizophrenia, and bipolar disorder (Belmonte *et al.* 2004; Ghosh *et al.* 2017). Many of these diseases are stress-related disorders (Nestler *et al.* 2002). Therefore, insights made using *C. elegans* may improve the understanding of multiple human illnesses (Baumeister 2002; Calahorro *et al.* 2010; Calahorro and Ruiz-Rubio 2011).

NMGP-1 protein is the GPM6A ortholog in the worm and is the only proteolipid protein family member in nematodes. To date only RNAseq experiments have characterized *nmgp-1* expression in larval *C. elegans* (Hammarlund *et al.* 2019; Cao *et al.* 2017). However, the adult expression patterns and the function of this gene remains unknown. We constructed a transcriptional reporter strain to establish the cellular and temporal patterns of *nmgp-1* expression. We report expression in the nervous system and in the egg-laying apparatus of adult hermaphrodites. To understand the role of *nmgp-1* in normal physiology, we characterized the anatomy and behavior of *nmgp-1(RNAi)*-treated animals and two *nmgp-1* mutant alleles. The two *nmgp-1* mutant alleles show defects in pharyngeal morphology. Neuronal knockdown of *nmgp-1* resulted in morphological changes in ASJ sensory neurons. Both mutant strains and RNAi treated worms showed altered egg-laying, augmented dauer recovery times and defects in chemorepulsion.

MATERIAL AND METHODS

C. elegans strains and culture conditions

C. elegans were grown on nematode growth media (NGM) plates streaked or spotted with live *Escherichia coli* OP50 at 21 °C. Nematodes were grown under standard conditions (Brenner 1974). Following behavioral assessments, plates containing worms were decontaminated using sodium hypochlorite 1 % and then discarded. Mutant strains were backcrossed four times according to the protocol of Fran Norflus and Claire-Anne Gutekunst (personal communication). The Bristol N2 reference strain (WB Cat# WBStrain00000001, RRID:WB-STRAIN:WBStrain00000001) obtained from the *Caenorhabditis* Genetics Center (CGC, USA) was used as the control strain. Potential *nmgp-1* mutant strains VC20170 (allele *gk144571*, from the Million Mutation Project) and *tm5483* were obtained from *C. elegans* Gene Knockout Lab, University of British Columbia (Vancouver, Canada) and the National Bioresource Project for the Experimental Animal "Nematode *C. elegans*" (Japan), respectively. *gk144571* (WBVar00367814) strain exhibits a G-to-A change at nucleotide 117 of exon 1 that introduces the non-synonymous mutation Met39Ile (arrowheads in Figure 1). *tm5483* (WBVar00600901) strain shows a deletion of 672 bases spanning part of exon 1 (including ATG codon), exon 2, introns 1 and 2 and part of exon 3 (grey box in Figure 1A). Both potential *nmgp-1* mutant strains were backcrossed to N2 to obtain MYM 001 [*nmgp-1(tm5483)*] and MYM 002 [*nmgp-1(gk144571)*], respectively. Because these mutant animals have many mutations, backcrosses were carried out to isolate the mutation of interest. To analyze ASJ neuron morphology, strain OE3010 ofEx4 [*trx-1::GFP + lin-15(+)*] was crossed to TU3595 (*uIs72 [pCFJ90 (Pmyo-2::mCherry) + Punc-119::sid-1 + Pmec-18::mec-18::gfp]; sid-1(pk3321); him-5(e1490) V; lin-15b(n744)*) (see below) to visualize ASJ neurons in the context of *nmgp-1(RNAi)*-treatment.

The *Pnmgp-1::GFP::unc-54 3'UTR* transcriptional reporter strain AVG14 was generated using the PCR-fusion method (Hobert 2002) to fuse the 1,694 bp 5' upstream promoter region of *nmgp-1* to GFP's coding sequence plus *unc-54* 3'UTR amplified together from the pPD95_75 plasmid (Addgene). The oligonucleotides used were: forward: 5'-GAG CTG AAT GAG CCA GGA AT-3', reverse: 5'-CGC CTC TTT CGT TGA TCT TG-3'. The construct (crude PCR fusion product, not plasmids) was injected into day 1 N2 animals at a concentration of 50 ng/µl, using *Pmyo-3::mCherry* as a red body wall co-injection marker at a concentration of 30 ng/µl. The same construct (50 ng/µl) and 50 ng/µl using *Pcoel::GFP* as green coelomocyte co-injection marker was used to inject the NeuroPAL strain (OH15500) to identify the neurons expressing *nmgp-1*. All strains generated are available upon reasonable request.

No ethical approval was needed for the study. The study was not pre-registered. No randomization was performed in this study. No statistical method was used to determine sample size. Sample size was arbitrarily set to a minimum of 30 animals per condition and/or strain in each assay as is standard in the field (Hughes *et al.* 2019; Yemini *et al.* 2021). In behavioral experiments, control and treated animals were assessed in parallel whenever possible. Otherwise, control animals were assessed prior to treated ones and then alternately. No blinding was performed in this study, except in microscopic observation of ASJ neurons (see below). Figure 2 shows a timeline including all of the experimental procedures carried out.

RNA interference (RNAi)

To induce RNA interference, we used the neuronally sensitive strain TU3595 [(*uIs72 [pCFJ90 (Pmyo-2::mCherry) + Punc-119::sid-1 + Pmec-18::mec-18::gfp]; sid-1(pk3321); him-5(e1490) V; lin-15b(n744)*)]. Neuronal expression of the RNA channel SID-1 in the TU3595 strain increases neural response to dsRNA (Calixto *et al.* 2011). Synchronized adult hermaphrodite worms were seeded on solid NGM medium supplemented with 1 mM IPTG, 50 μg/ml ampicillin and fed with the HT115 strain with the L4440 vector encoding the complete *nmgp-1* ORF (clone F13H8.4, Open Biosystems, MA, USA). RNAi phenotypes were analyzed in the F2 (Figure 2A). As control, worms were fed with the bacterial strain HT115 with the L4440 vector encoding no ORF. To analyze ASJ neuron morphology in worms treated with *nmgp-1(RNAi)*, hermaphrodites OE3010 were crossed four times with males from the TU3595 RNAi sensitive strain. Worms were selected by GFP expression on ASJ neurons, on touch receptor neurons (TRN) and by mCherry on pharyngeal muscle cells.

Bioinformatics analysis

We analyzed the NMGP-1 sequence to describe its putative structure and to identify the conserved motifs. We used the BLASTp tool from NCBI to determine similarity among *M. musculus* GPM6A, *D. melanogaster* M6 and NMGP-1 from *C. elegans*. Secondary structure and solvent accessibility were predicted with the NetSurfP server (Petersen *et al.* 2009) (www.cbs.dtu.dk/services/NetSurfP/). Parameters for wild-type and mutant NMGP-1 were compared. We used the TMHMM server 2.0 (CBS Prediction Servers, www.cbs.dtu.dk/services/TMHMM/) to analyze NMGP-1 primary sequence and to predict transmembrane helices. In addition, protein motifs were predicted with PredictProtein Server (Rost *et al.* 2004), which includes PHD predictions for protein topology, PROF predictions for motif scan (PROSITE, including those

motifs with a high probability of occurrence) and DISULFIND for disulfide bridge prediction. Finally, the SNAP tool was used to predict the functional effects of single amino acid substitution on NMGP-1 (Bromberg *et al.* 2008).

Cloning and Plasmids used

nmgp-1 coding sequences from N2 wild-type and MYM 002 [*nmgp-1(gk144571)*] strains were cloned into pEGFP-C1 vector (BD Biosciences Clontech, US) to generate wild-type and mutant NMGP-1 proteins fused to the green fluorescent protein (GFP). We designed primers to amplify the complete coding sequence of *nmgp-1*. *BamHI* and *XhoI* restriction site sequences were added. Oligonucleotide sequences used were: 5'-CTC GAG ATG ATG TCC TGG GCA TTT AAT G-3', forward primer and 5'-GGA TCC TTA GTA AAC CGG TTT TAA TCT TTT ATC 3', reverse primer. Both wild-type and mutant NMGP-1 were cloned to the C-terminus of EGFP (C-terminal fusions). As controls, the following plasmids were used: GFP-PH (plasmid 21179, Addgene, Cambridge, MA, USA) that binds to plasma membrane phospholipids and is found enriched at the plasma membrane (Stauffer *et al.* 1998) and GFP::GPM6A (Alfonso *et al.* 2005).

Cell line culture and Transfections

COS-7 cells (ATCC® CRL-1651; RRID:CVCL_0224, maximum number of passages: 30. This cell line is not listed as a commonly misidentified cell line by the ICLAC. No further authentication was performed in the laboratory.) were cultured in DMEM with 10 % v/v fetal bovine serum, penicillin, and streptomycin. For transfections, we used polyethylenimine (PEI, School of Pharmacy and Biochemistry, UBA, Buenos Aires, Argentina). Briefly, 2 µg of plasmid DNA and 3 µl of 25 mM PEI were diluted in 50 µl of protein and antibiotic free medium (OPTI-MEM I Reduced Serum Medium, Invitrogen, Argentina) and incubated for 8 minutes. Then, 200 µl of complete medium were combined with the transfection mix and added to each well in a 24 wells per plate format, containing cells previously washed twice with phosphate buffered saline (PBS). Cells were incubated with the transfection mix for 2 hours at 37 °C. Cells were then washed and the medium was replaced by fresh complete medium.

Cell staining and Image analysis

Twenty-four hours after transfection, COS-7 cells were fixed and stained with rhodamine phalloidin 1/1000 (Thermo Fisher Scientific Cat. no.#R415, RRID:AB_2572408, US) as previously described (Fernández *et*

al. 2010). Nuclei were stained with 4'-6-Diamidino-2-phenylindole (DAPI, Molecular Probes). Fluorescent images were acquired using a Nikon E600 microscope equipped with epifluorescence illumination (Nikon, Japan) with an 100x oil-immersion lens or a confocal laser scanning microscope (Olympus FV-300 - Olympus Bx-61, with a 63x/1.4 objective, Melville, NY USA). Confocal microscopy sections were acquired in sequential mode using FluoView software (v 3.3, Olympus). Four optical sections were obtained (z-step = 0.5 µm). Images were processed using Photoshop 8.0.1 (Adobe Systems). Plot profiles of fluorescence intensity were generated using ImageJ software (plot profile tool).

We calculated the percentage of cells displaying filopodial protrusions (visualized by the F-actin marker phalloidin) for both transfected as well as non-transfected cells from the same coverslip. We then determined the ratio of transfected to the non-transfected filopodium-bearing cells from the same coverslip (assay endpoint). In total, 120-135 cells were analyzed in each experiment from three independent transfection assays. Each experiment consisted of 3 technical replicas that included 40-45 cells per coverslip.

Lifespan analysis

Lifespan was determined at 21 °C. To obtain a synchronized population, adult hermaphrodite worms were allowed to lay eggs for 2 h (Figure 2A). Then parental worms were discarded and eggs were maintained until hatched embryos become adults. Lifespan was monitored from the first adult day (Figure 2B). During the fertile period (i.e., the first week), adult worms were carefully transferred to fresh plates to avoid mixing two generations. We did not supplement medium with fluorodeoxyuridine (often used to prevent the population from producing progeny (Youngman *et al.* 2011) because this reagent can extend the lifespan of short-lived strains according to Anderson et al. (2016). We recorded the number of surviving animals (assay endpoint) 6 days a week and scored plates for survivors. Animals were considered dead when they failed to respond to touch by an eyelash and/or pharyngeal pumping was not present. In total, 30-60 animals from at least 3 independent plates per strain were tested. Worms with the bag-of-worm phenotype were excluded from the lifespan assay. Lifespan curves represent the percentage of living worms as a function of time. For statistical analysis, the mean lifespan of each strain was calculated as the time (in days) at which 50 % of the starting population is still surviving.

Egg-laying

Egg-laying was analyzed in liquid M9 medium in the presence or absence of 35 mM serotonin.

Serotonin stimulates egg-laying in liquid by simulating the activity of the serotonergic HSN neurons which innervate egg-laying muscles and deliver serotonin to activate them (Hardaker *et al.* 2001). Eight adult hermaphrodite worms per condition (2-3 days old, with visible eggs in their uteri, Figure 2B) were allowed to lay eggs for 60 min at 21 °C. The number of eggs laid (at the assay endpoint) was counted. Each condition (with or without serotonin), consisted of four-five replicas (i.e., 4 independent plates) so that 64 worms per strain were assayed. No exclusion criteria were predetermined.

Levamisole assay

Individual day 2-3 hermaphrodite adults (Figure 2B) were placed in a 96 microtiter well plate. Five to ten animals per strain and condition from 5 independent plates were assayed (i.e., 20-50 animals per strain). Worms were separated into 4 to 10 individuals/well. Each well contained liquid M9 without serotonin and the indicated concentration of levamisole (0, 5, 10, 25 and 50 µM; Sigma Aldrich, CAS number 16595-80-5). After 1 hour the number of laid eggs (assay endpoint) was recorded. The count per well was normalized by the number of worms per well. No exclusion criteria were predetermined.

Measurement of dauer recovery time

Entrance to the resistant dauer stage was induced by starvation and overcrowding. Adult hermaphrodite worm cultures were grown for an additional 4-5 days after food was finished (Figure 2B). Cultures were incubated in 1 % sodium dodecyl sulfate (SDS), which eliminates all non-dauer individuals and eggs, to isolate dauer larvae (Karp 2018). To evaluate recovery from the dauer state and re-entry into the life cycle, dauer larvae were transferred to fresh plates with an OP50 spot and incubated at 21 °C until L3/L4 larvae were observed (primary assay endpoint). The time to recover (i.e., to pass to the L4 stage) was recorded. Recovery curves represent the percentage of dauer larvae as a function of time. The mean recovery of each strain was calculated as the time (in hours) at which recovery reached 50 % of the starting population. For control N2 and mutants MYM001 [*nmgp-1(tm5483)*] and MYM002 [*nmgp-1(gk144571)*], a total of 30-45 dauer larvae from 3 independent original plates overcrowded to induce dauer formation were analyzed. For worms treated with *nmgp-1(RNAi)*, 55-130 dauer larvae from 2 - 7 independent original plates overcrowded to induce dauer formation were analyzed. Those dauer larvae that did not move were recorded as dead and were excluded from assay.

Chemotaxis assay

Staged young adults (obtained by growing the progeny of bleached gravid adults) (Porta-de-la-Riva *et al.* 2012) were used for chemotaxis assays (Figure 2A, B). Attraction to diacetyl and avoidance to SDS were assessed in quadrant assays, as described (Matsuura *et al.* 2013). Briefly, a 10-cm-diameter tissue culture dish containing 0.001 M $CaCl_2$, 0.001 M $MgSO_4$, 0.2 M KH_2PO_4 buffer, 0.5 mg/ml cholesterol and agar was divided into four quadrants. In two opposed quadrants, the compound of interest is placed and in the other two, the S basal buffer. Worms were washed 3-5 times with S basal buffer and then placed in the center of the plate and left to move freely on the assay plate for 1h. In total 30-90 were tested, i.e., 15-30 nematodes/strain were placed at the initial location. Thus, each strain was tested from at least three independent plates. For the attraction assay, 2 µl 0.5 % (v/v) diacetyl in the S basal buffer was spotted. For the avoidance assay, 2 µl 0.1 % (w/v) SDS in the S basal buffer was spotted. As a control, 2 µl S basal buffer was spotted. Sodium azide (0.25 M) was included in each spot to immobilize worms. Under a microscope, the number of worms at each quadrant (assay endpoint) was recorded. Worms that remained in origin (center of the plate) or in the quadrant boundaries and that were not anesthetized were excluded from the assay. We calculated chemotaxis (C.I.) and avoidance indexes (A.I.) (number of animals at test quadrant - number of animals at control quadrant)/(total number of animals on plate).

Microscopic observation

For confocal images, adult worms (Figure 2) were carefully picked up and transferred to fresh 2 % agar pads, anesthetized with 0.2 M sodium azide and then covered with a coverslip.

Images were acquired with a confocal laser scanning microscope (Olympus FV-300 - Olympus Bx-61, with a 63x/1.4 objective, Melville, NY USA). Images were acquired in sequential mode with the FluoView (version 3.3, Olympus) and processed with Fiji software (ImageJ 1.52g).

ASJ neurons in worm heads expressing GFP were observed. When abnormalities (blebs in loops or dendrites, disrupted dendrites) were detected in any of these cells, worms were considered defective. The number of defective worms was the assay's primary endpoint. We observed more than 100 animals per strain from at least 4 independent plates (105 individuals for control and 133 for *nmgp-1(RNAi)*-treated individuals). During microscopic observation of ASJ neurons, the investigators were blind to the genotype. Animals were identified by coded names assigned to each genotype, which were announced to the investigator only after finishing observation.

A similar protocol was used for visualization of pharynx defects and bag-of-worm phenotype. The number of worms with pharynx defects or with late embryos were the assay primary endpoints, respectively. DIC images were acquired for worm analysis. More than 170 (177-254) worms per strain distributed from at least 6 independent plates were observed.

Statistical data analysis

Graphs and statistical analysis were done with GraphPad Prism 6.0 software (RRID:SCR_002798). Assessment of the normality (Shapiro–Wilk test) of the data and test for outliers (Grubbs' test) was performed. Group means were analyzed for overall statistical significance by one-way ANOVA followed by multiple comparison tests. Non-parametric analysis was performed (Mann-Whitney or Kruskal-Wallis followed by multiple comparison tests) when assumptions on the normal distribution were not met. Statistical analysis for lifespan and *dauer* recovery data were carried out using a Log-rank (Mantel-Cox) curve comparison. In all figures, plotted data represent media from independent plates.

RESULTS

Comparison of the NMGP-1 tertiary structure to GPM6A

The *nmgp-1* gene (WBGene00017437, sequence: F13H8.4) of *C. elegans* maps on the plus strand of chromosome II. The complete *nmgp-1* structure comprises 6 exons (Figure 1A). While Wormbase predicts one transcript, AceView Wormgenes (Thierry-Mieg and Thierry-Mieg 2006) annotated mRNA sequence browser identifies four different mRNA variants. One of them corresponds to the full-length transcript and two other variants contain sequences coding the C-terminus. The remaining variant appears to not encode a functional protein (Thierry-Mieg and Thierry-Mieg 2006).

The full-length transcript produces the protein NMGP-1 (NP_495253.2, UniProtKB Q19430), which is comprised of 275 amino acids. A Position-Specific Iterated BLAST (PSI-BLAST) analysis comparing the *C. elegans* NMGP-1 against a non-redundant protein sequence (nr) database revealed a high identity with NMGP-1 from many free-living nematodes or parasitic roundworms (i.e., *Caenorhabditis brigssae*, *Brugia malayi*, *Pristionchus pacificus*, etc.). We also compared similarity between *C. elegans* NMGP-1 and *D. melanogaster* M6 (isoform A, AFD28985.1) and between the three mouse PLP proteins: GPM6A (AAH23461.1), GPM6B (P35803) and PLP1 (P60202.2). Because worms and flies express only one PLP protein, we compared them and found that NMGP-1 and *D. melanogaster* M6 share 24% identity and 48% similarity

(Figure 1B). Alignment with PLP1 showed 22% identity and 44% similarity; however, less than 35% of NMGP-1 amino acids aligned with the PLP1 sequence. In contrast, comparisons with mouse GPM6A and GPM6B included 57% and 78% of NMGP-1 amino acids, respectively. Nevertheless, NMGP-1 and GPM6B share only 19% identity and 37% similarity. These percentages were slightly higher for GPM6A (21 and 43%, respectively; Figure 1B), suggesting that NMGP-1 could be orthologous to both GPM6A and GPM6B, although more similar to GPM6A. Accordingly, the ortholist of Greenwald's database (Shaye and Greenwald 2011) shows *nmgp-1* as the sole ortholog of *gpm6a*.

We used the program TMHMM (Denmark University) (Krogh *et al.* 2001) to predict transmembrane helices and topology of these proteins. Predictions for NMGP-1 indicate that similarly to M6, GPM6A and other proteolipidic proteins, it contains transmembrane domains (red boxes in Figure 1B,C) and the C-terminus is located in the cytoplasm. However, instead of the four transmembrane regions typically observed in mammalian GPM6A and *D. melanogaster* M6, NMGP-1 displays only three. As a consequence, and unlike GPM6A and M6, the N-terminus of NMGP-1 is located in the extracellular space (Figure 1C,D), a common feature among *C. elegans* transmembrane proteins (Krogh *et al.* 2001). Sequence comparison (Figure 1B) indicated that the first NMGP-1 transmembrane domain aligns to the second transmembrane domain in *D. melanogaster* M6 (red boxes in Figure 1B).

Next, we looked for putative target sites for posttranslational modifications within the NMGP-1 sequence. We found putative N-glycosylation, myristoylation and C-palmitoylation sites (white and black triangles and white circle in Figure 1D) and identified casein kinase 2 (CK2) and protein kinase C sites (white and black squares in Figure 1D). Despite the lack of identity between C-terminal domains of M6 or GPM6A and NMGP-1, phosphorylation sites detected in the C-terminal of NMGP-1 correspond to the phosphorylation sites present in the C-termini of the mouse and the fly proteins, suggesting a conserved regulation through phosphorylation for PLP proteins. Tyrosine 229 (highlighted Y in Figure 1B and grey box in Figure 1D) is also conserved and corresponds to Y251 of mouse GPM6A. Phosphorylation of this residue is required for neurite outgrowth (Formoso *et al.* 2015a). NMGP-1 also contains 4 cysteine residues (highlighted Cs in Figure 1B and black circles in Figure 1D) in its only extracellular loop. Interestingly, the role of GPM6A in filopodium outgrowth requires the major extracellular loop, which is maintained through two disulfide bridges formed by four cysteine residues (Fuchsova *et al.* 2009). Similarly, the cysteine residues in NMGP-1 may maintain the loop.

Similar to GPM6A, NMGP-1 promotes filopodium formation

We next examined the subcellular localization and the biological function of NMGP-1. Mammalian COS-7 cells (with no detectable GPM6A expression) were transfected with the plasmids to overexpress the following GFP fusion proteins: worm NMGP-1, mouse GPM6A and GFP-PH as a control that localizes GFP signal to the plasma membrane (Figure 3A). As already shown, GPM6A localizes in the cell membrane (Fuchsova *et al.* 2009). NMGP-1 also appeared to localize on the cell surface (arrowheads in Figure 3A). Furthermore, a line scan measuring GFP intensity across the cell showed peaks consistent with plasma membrane localization (Figure 3C), indicating NGMP-1 presence on the plasma membrane. Mammalian GPM6A, GPM6B, DM20 and *D. melanogaster* M6 overexpression induces filopodium (or membrane protrusion) formation in neuronal and non-neuronal cells (Alfonso *et al.* 2005; Fernández *et al.* 2010; Zappia *et al.* 2012). To evaluate if this function was conserved in NMGP-1, we measured filopodium formation in mammalian COS-7 cells. NMGP-1 overexpression increased the formation of membrane protrusions when compared with control cells (one-way ANOVA $F(3, 18)= 45.29$ with Tukey's multiple comparison test, $n = 3$ independent cultures, $p<0.0001$, Figure 3D). In addition, NMGP-1 induced filopodium outgrowth to a similar extent as did mammalian GPM6A (Figure 3A, black arrows). These results support the idea that NMGP-1 is functionally conserved.

To gain insight into *in vivo* NMGP-1 function, we analyzed the phenotypes of the mutant worm strain MYM 002 [*nmgp-1(gk144571)*] (see below). Genotyping of this strain showed a non-synonymous Met39Ile mutation (arrowheads in Figure 1A,D and black box in Figure 1B). The coding sequence of this mutant NMGP-1 (mutNMGP-1) was cloned and its subcellular localization and ability to induce filopodium formation were evaluated in COS-7 cells. mutNMGP-1 localized preferentially inside the cell, with enrichment in the perinuclear zone (white arrows in Figure 3A,B). Accordingly, the plot profile for the mutNMGP-1-expressing cell shows a higher intensity inside the cell (Figure 3C). We next evaluated its ability to form membrane protrusions. In contrast to wild-type NMGP-1, the mutNMGP-1 did not induce filopodium formation (Figure 3A,D, $n = 3$ independent cultures, GFP vs. mutNMGP-1, unpaired t-test $t(9)=1.558$, $p<0.4$. NMGP-1 vs. mutNMGP-1, unpaired t-test $t(10)=10.67$, $p<0.03$). These results suggest that the M39I mutation may alter protein structure, inducing NMGP-1 delocalization and resulting in subsequent loss of function.

***nmgp-1* expresses mostly in sensory neurons and in the egg-laying apparatus**

To determine *nmgp-1*'s pattern of expression, we built the transcriptional reporter strain AVG14 (*Pnmgp-1::GFP::unc54_3'UTR*). To this end, we selected the ~1.6 kb region immediately upstream of the start codon of the gene, including the predicted promoter and the putative enhancer regions. This region was used to drive expression of green fluorescent protein (GFP) via PCR fusion. (Hobert, 2002). GFP expression driven by the putative *nmgp-1* promoter was detected in several cells, primarily neurons (Figure 4). Within the head (Figure 4A), we saw GFP expression in pharyngeal neurons, as many somas and processes within the metacorpus and the posterior bulb ventral ganglia were observed. In addition, some of the processes next to the bulb might correspond to CEP sheath glial cells. In the midbody, we saw labelling of cells within the egg-laying apparatus (Figure 4B). Posteriorly, we observed cells in the tail ganglia and possibly phasmid neurons (Figure 4C). Neuronal processes along dorsal and ventral cords were also labelled (Figure 4D). In addition, to identify specific neurons, we used the NeuroPAL strain (OH15500) developed by Hobert's Lab (Yemini *et al.* 2021). This strain has a stereotyped fluorescent color map to identify all neurons. We injected it with the same plasmid for GFP expression under the *nmgp-1* promoter. Figure 4E-G shows images of the head, midbody and the tail. The following neurons were identified as expressing GFP: ALA, CEPD, IL1 (head neurons from the nerve ring), the sensory amphid neurons ASK, neurons from the anterior ventral nerve cord (VA6, VB7, DB5, AS5, VD6, DD3, DA4) and posterior ventral cord (VA11, VD11, AS10, DA7, DB7, CB11, VA11), neurons from the preanal ganglion (PVP, PVT, DD6, AS11, VA12, DA8, DA9) dorso-rectal ganglion (DVB, DVA, DVC) and lumbar ganglion (PVQ, PHC). The neurons identified include sensory neurons (amphid and mechanosensory), motor neurons and interneurons.

To gain insight into *nmgp-1* function in worms, we quantified lifespan, dauer recovery and egg-laying in two *C. elegans nmgp-1* mutants. We chose lifespan quantification as a general behavior, dauer recovery as a measure of the worm's ability to detect stress cessation and egg-laying based on *nmgp-1*-reporter expression in the egg-laying apparatus. One strain, MYM 001 [*nmgp-1(tm5483)*] has a 672 bp deletion comprising part of exon 1, exon 2, part of exon 3 and introns 1 and 2 (grey shadow in Figure 1A, B, D). The other strain is MYM 002 [*nmgp-1(gk144571)*] with a non-synonymous Met39Ile mutation, which lies within the first transmembrane domain (Figure 1D). According to the Ensembl's Variant Effect Predictor, this variant has a medium severity of impact on the protein sequence. Morphological examination of mutant worms showed visible changes in the pharynx. Mutant worms showed irregular pharynx morphology, with bent procorpus and isthmus rather than straight as in wild-type N2 worms (figure 5A,B; 21.7 ± 3.2% for MYM001 and 19.4 ± 5.8% MYM002 vs. 3.1 ± 1.4% for N2; $p<0.0001$ and $p<0.0039$, respectively; Kruskal–Wallis one-way ANOVA

followed by Dunn's multiple comparison tests for *post hoc* effects). In rescue assays, injection of the wild-type *nmgp-1* gene including upstream regulatory regions into MYM 001 [*nmgp-1(tm5483)*] and MYM 002 [*nmgp-1(gk144571)*] mutants reversed the pharyngeal morphological defects associated with this strain (Supplemental Figure 3A,B; p<0.23, Kruskal–Wallis one-way ANOVA followed by Dunn's multiple comparison tests for *post hoc* effects).

Locomotor activity of mutant worms was analyzed by assessing the movements of hermaphrodite worms on a solid medium. Mutant worms moved in a wild-type like manner and showed no obvious uncoordinated phenotype (Suppl. Figure 1). Since many aspects of *C. elegans* behavior are dependent on locomotion, these results allowed us to rule out the possibility that subsequent differences in other phenotypes could be due to locomotor deficits.

We next evaluated life span under physiological conditions. The life span at 21 °C of MYM 001 [*nmgp-1(tm5483)*] and MYM 002 [*nmgp-1(gk144571)*] strains was compared to that of N2 (control) hermaphrodite worms. Control worms showed a maximal life span of 19 days (Figure 5C). Both *nmgp-1* mutants had significantly shorter maximal lifespans (16-days, Log-rank (Mantel-Cox) test Chi square 3.895, n = 3-5 independent plates, p<0.1, Figure 5C). Mean lifespan (i.e., the time in which half of the population has died) for MYM 001 [*nmgp-1(tm5483)*] mutant was similar to N2 worms, but it was lower for MYM 002 [*nmgp-1(gk144571)*] mutant (9.7 ± 0.7 and 7.2 ± 0.2 days for MYM 001 [*nmgp-1(tm5483)*] and MYM 002 [*nmgp-1(gk144571)*] respectively vs. 9.3 ± 0.6 for N2 worms, Kruskal-Wallis statistics 6.331, n = 3-5 independent plates, p<0.03, dashed line in Figure 5C). Differences between mutants suggest that the Met39Ile mutation in the MYM002 [*nmgp-1(gk144571)*] strain is more deleterious for lifespan than the loss of more than an entire exon in the MYM001 [*nmgp-1(tm5483)*] strain.

To test if the lifespan reduction observed in mutant *nmgp-1* worms is due to disruptions in the nervous system, we used RNAi feeding to reduce neural expression of *nmgp-1* in the strain TU3595. This strain pan-neuronally expresses the dsRNA channel SID-1, increasing the response of neurons to dsRNA (Calixto *et al.* 2011). Compared to TU3595 control fed bacteria with empty vector, animals fed bacteria to induce *nmgp-1(RNAi)* had *nmgp-1* mRNA levels reduced by 70 % (Mann-Whitney U test 1.50, n = 4-6 independent plates, p<0.003, Suppl. Figure 2).

Lifespan at 21 °C of *nmgp-1(RNAi*)-treated worms was compared with that of TU3595 (control) worms. We found no statistical difference between either the maximal or mean lifespan of control-TU3595 worms and that of *nmgp-1(RNAi)* animals. (Control maximum lifespan = 12 days vs. *nmgp-1(RNAi)* = 11 days, Log rank

(Mantel-Cox) test Chi square 0.8727, p>0.3; mean lifespan control = 7.4 ± 0.5 vs. *nmgp-1(RNAi)* = 6.0 ± 0.8, unpaired t test t(12)=4.569, p>0.1; 6 independent plates, dashed line in Figure 5D).

Next, we studied the effect of *nmgp-1* mutations on dauer recovery. Dauer entry and recovery are mediated by the appropriate detection and integration of environmental signals. Under adverse and stressful conditions, *C. elegans* can develop into dauer larva, a life-stage specialized for survival. During dauer stage, animals become stress resistant. When favorable conditions are reestablished, dauer larvae reenter the life cycle and continue with normal development (Hu 2007). To assess the necessity of normal *nmgp-1* function for dauer recovery, we quantified the time dauer larvae took to reach L3/4 larval stage upon reintroduction of food. Dauer formation was induced by starvation and overcrowding (Karp 2018). L3/4 larvae were identified by morphological changes and the resumption of pharyngeal pumping. N2 wild-type dauer larvae exhibited complete recovery in 20 h (Figure 5E). Dauer larvae from both mutant strains recovered significantly slower than controls (21 h in both cases, Log-rank (Mantel-Cox) Test Chi square 7.21, p<0.03; Figure 5B). Mean recovery time (when 50% of the animals have recovered) for both mutant strains increased when compared to N2 worms (14.3 ± 0.3 vs. 15.0 ± 0.7 for MYM 001 and 16.3 ± 0.6 for MYM 002, Kruskal-Wallis statistics 5.23, n = 3 independent plates, p<0.077, Figure 5E). Although p value does not show statistical significance (probably due to asymmetric data distribution), Dunn's multiple comparisons test indicated a significant difference between mean recovery times for N2 and MYM 002 [*nmgp-1(gk144571)*]. These results suggest that this mutation could subtly affect dauer recovery.

Since dauer recovery depends on neural activity, we used neuronal RNAi (TU3595 strain) to assess if neural expression of *nmgp-1* is required for dauer recovery. Starvation and overcrowding induced dauer larva development to a similar extent in control and *nmgp1(RNAi)*-treated worms (data not shown). However, while control worms recovered after 5 h, recovery of the dauer larvae of *nmgp-1(RNAi)* worms was significantly delayed (18 h, Log-rank (Mantel-Cox) Test Chi square 260.0, p<0.0001; Figure 5F). The mean recovery time (when 50 % of the animals have recovered) also significantly increased for *nmgp-1(RNAi)*-treated worms (4.3 ± 0.1 vs. 16.2 ± 0.1 for RNAi, Mann Whitney U test, two-tailed n = 4 independent plates p<0.03; dashed line in Figure 5F). These results suggest that *C. elegans* requires normal neuronal *nmgp-1* levels for timely dauer recovery.

It should be noted that in the RNAi assays, worms were fed HT115 bacteria carrying the RNAi plasmid either with *nmgp-1* ORF (test) or without *nmgp-1* ORF (control). However, in experiments comparing wild-type (N2) and *nmgp-1* mutant worms, animals were fed OP50 bacteria. Beyond the obvious difference

between the genetic backgrounds of N2 and TU3595 worms, the different nutritional and other characteristics between these bacterial strains may explain disparities in lifespan and dauer recovery between experiments (Shtonda and Avery 2006; Urrutia *et al.* 2020). We induced dauer exit in N2 worms with HT115 and in TU3595 worms withOP50 to test if bacterial strain modifies dauer recovery time. Dauer larvae from N2 worms fed HT115 recovered after 5-6 h (Supplementary Figure 4A), similarly to TU3595 fed with the same bacterial strains (Figure 5F). By contrast, dauer larvae from TU3595 strain fed OP50 showed a recovery time of 15-16 h (Supplementary Figure 4B), similarly to the mean time obtained for N2 fed OP50 (Figure 5E). These findings confirm the hypothesis that bacterial strains influence dauer recovery.

***nmgp-1* mutations affect egg-laying and induce bag-of-worm phenotype**

After detecting *nmgp-1* reporter expression in the egg-laying apparatus, we analyzed egg-laying in *nmgp-1* mutants. Egg-laying is modulated by the HSN motor neurons, which secrete serotonin to activate the muscles responsible for egg deposition (Brewer *et al.* 2019). We quantified the serotonin-induced egg-laying rate of mutant strains and compared it to that of N2 control worms. Without serotonin, there were no differences between egg-laying rates in *nmgp-1* mutants and N2 control worms. However, under serotonin stimulation, MYM 001 [*nmgp-1(tm5483)*] and MYM 002 [*nmgp-1(gk144571)*] worms showed a significantly reduced number of eggs laid with respect to N2 control animals. N2 worms laid on average 17 eggs/h, while both mutant worms laid approximately 7 eggs/h (one-way ANOVA $F(5,39) = 11.42$ with Brown-Forsythe post hoc test, n = 5 independent plates, $p<0.0001$, Figure 6A). In rescue assays, when stimulated with serotonin, both MYM 001 *[nmgp-1(tm5483)]* and MYM 002 *[nmgp-1(gk144571)]* mutants injected with the wild-type *nmgp-1* transgene showed an increase in egg-laying rate similar to N2 worms (Figure 6G). This suggests that *nmgp-1* is required for serotonin-induced egg-laying in *C. elegans*. These results were further supported by egg-laying assays with *nmgp-1(RNAi)*-treated worms (neuronal RNAi). In the absence of serotonin, both control and *nmgp-1(RNAi)* worms in M9 laid approximately 1-2 eggs/h, similarly to the previously reported rates for N2 wild-type worms (Carnell *et al.* 2005) (Figure 6B). Under serotonin stimulation, egg-laying in controls increased significantly to about 11 eggs/h ($p<0.01$, Figure 6B). We found that *nmgp-1(RNAi)*-treated worms also showed a significant increase in egg-laying in response to serotonin treatment (2-5 eggs/h); however, this increase was significantly smaller than in RNAi control worms (Kruskal-Wallis statistics 13.43 with Dunn's multiple comparisons test, n = 4 independent plates, $p<0.0001$, Figure 6B). These results suggest that reduced neuronal expression of *nmgp-1* may affect the serotonin-responding cells involved in egg-laying.

Worms defective in egg-laying usually show egg retention (known as the "bag-of-worm" phenotype). Egg retention leads to intra-uterine hatching and larval development inside the parental body. We therefore quantified the incidence of bag-of-worm phenotype among mutant worms. In both mutants, we observed a higher occurrence of retention of late-stage embryos (comma, twofold or pretzel stage; arrowheads in Figure 6Cii and 6Ciii, compared to N2 controls, 6Di). Stacked bars in Figure 6E show the percentage of worms with late embryos or larvae in their uteri. MYM 001 [*nmgp-1(tm5483)*] had significantly more retained late embryos and larvae than N2 control (Kruskal-Wallis statistics 11.17 with Dunn's post hoc test, n = 10 independent plates, $p<0.003$, Figure 6E). Some late-stage embryo and larvae were also observed in *nmgp-1(RNAi)*-treated worms though difference was not statistically significant (Unpaired t test $t(25)=1.540$, $p>0.13$ n = 2 independent plates, Figure 6D and F). These observations suggest that neuronal wild-type *nmgp-1* may be necessary to prevent embryo retention. In rescue assays, MYM 002 [*nmgp-1(gk144571)*] mutants injected with the wild-type *nmgp-1* transgene had a significant reduction in the percentage of worms with the bag-of-worm phenotype (Supplemental Figure 3C).

Decreased response to serotonin-induced egg-laying could be related to defects in vulval muscles and/or neurons (Schafer 2006). To evaluate these possibilities, we quantified egg-laying frequency in *nmgp-1* mutants in a levamisole dose-response assay (in the absence of serotonin). Levamisole is a cholinergic agonist that selectively activates acetylcholine ion channel receptors in nerves and muscles (Trent *et al.* 1983; Kim *et al.* 2001). We counted the number of eggs laid in response to increasing concentrations of levamisole after 1 hr. We found no difference in levamisole-induced egg-laying between control (N2) animals and *nmgp-1* mutants (Figure 6G, two-way ANOVA, comparing main column effect, followed by Tukey's multiple comparisons test; interaction $F = 0.8952$, $p = 0.1539$; strain effect $F = 3.498$, $p = 0.1803$. n = 5 to 10 worms in five independent plates). These results suggest that vulval muscles and cholinergic neurons do not mediate the egg-laying phenotype of *nmgp-1* mutants.

nmgp-1 is required for normal sensory neuron morphology

Environmental stimuli leading to dauer recovery are largely detected by ASJ sensory neurons (Bargmann and Horvitz 1991). We generated a neuronal RNAi sensitive strain with ASJ neurons expressing GFP (TU3595 x OE3010) to analyze ASJ morphology in worms with reduced *nmgp-1* neuronal expression. ASJ neurons in most control animals appeared healthy, with dendrites projecting to the mouth in a continuous and almost straight line (arrows in Figure 7A, left panel). However, many *nmgp-1*-silenced worms had ASJ

projections with significant impairments including blebs or processes that failed to reach the buccal cavity (arrowheads in Figure 7A right panel, Supplemental Figure 5; unpaired t test $t(9)=3.287$, $p<0.005$ n = 5-6 independent plates, Figure 7B). These results suggest that *nmgp-1* is necessary for normal ASJ morphology. Furthermore, impairments in ASJ morphology could lead to altered environmental sensation and the delays observed in worms with reduced *nmgp-1* neuronal expression.

To assess if *nmgp-1* is required for additional chemosensory functions, we performed attraction and avoidance (chemotaxis) assays with *nmgp-1* mutants and RNAi-mediated reduction of *nmgp-1* neural expression. Worms were exposed to compounds sensed by known and different groups of sensory neurons. First, mutants and control worms (N2) were tested for chemotaxis to the classical attractant compound diacetyl (Bargmann *et al.* 1993). In all cases, mutant and N2 worms were attracted to diacetyl spots (Kruskal-Wallis statistics 0.2257 with Dunn's post hoc test, n = 3-5 independent plates, $p>0.9$, Figure 7C), indicating that *nmgp-1* mutations did not affect this response. Similarly, *nmgp-1(RNAi*)-treated worms (with reduced *nmgp-1* neural expression) exposed to diacetyl were attracted to the spots similar to untreated worms (Mann-Whitney test, $p>0.6$, n= 3 independent plates, Figure 7D).

We next tested the avoidance response to the detergent SDS (Hilliard *et al.* 2002). When adult control worms were exposed to SDS, they stopped moving forward and started moving backward avoiding SDS spots. Adult MYM 002 [*nmgp-1(gk144571)*] behaved like control worms (Figure 7E). However, adult MYM 001 [*nmgp-1(tm5483)*] worms failed to move backward and even moved towards the SDS spot (ANOVA $F_{2,25}=4.067$, with Tukey's multiple comparison test, n = 4 independent plates, $p<0.03$, Figure 7E). Avoidance assays performed with *nmgp-1(RNAi)*-treated worms (with reduced *nmgp-1* neural expression) recapitulate these results (Unpaired t-test $t(13)=2.173$, $p<0.05$ n = 3 independent plates, Figure 7G), suggesting that sensory neurons responsible for avoidance behavior may be affected by *nmgp-1* reduction. Interestingly, larvae from MYM 001 [*nmgp-1(tm5483)*] showed a significant non-avoidance behavior (ANOVA $F_{2,33}=7.423$, with Bonferroni's multiple comparison test, n = 5-6 independent plates, $p<0.02$, Figure 7F) like adult worms. In the case of MYM 002 [*nmgp-1(gk144571)]* strain and *nmgp-1(RNAi)* treated larvae (Figure 7F, I), avoidance behavior was not statistically significant from controls. To further correlate the defects in the ASJ neurons with the avoidance behavior, we selected normal control and defective *nmgp-1(RNAi)*-treated worms and assayed for avoidance to SDS. In comparison to normal control worms, defective worms did not avoid the SDS (Unpaired t test $t(9)=3.455$, $p<0.007$ n = 4-7 independent plates, Figure 7I). To investigate if *nmgp-1* is

required for mechanosensory function, we performed touch assays and found that neither mutant displayed touch impairments (Supplemental Figure 6).

We have summarized our findings in Table 1. Phenotypic changes observed for *nmgp-1(RNAi)*-treated worms complemented those obtained for *nmgp-1* mutant strains. Conservatively, both approaches indicate that normal *nmgp-1* expression is required in *C. elegans* for proper egg-laying, dauer recovery and SDS avoidance.

Table 1. Summary of phenotypic changes observed in worms with altered *nmgp-1*

Test/Assay	MYM001	MYM002	Neuronal RNAi
Filopodium induction	ND	**X***	ND
Mean life span	ok	**X**	ok
Dauer entrance (qualitative)	ok	ok	ok
Mean recovery time for dauer exit	**X**	**X**	**X***
Egg laying	ok	ok	ok
Egg laying with 5HT	**X**	**X**	**X**
Advanced embryos in uterus	**X**	ok	**X**
Egg laying with levamisole (no 5 HT)	ok	ok	ND
Defects in ASJ morphology	ND	ND	**X***
Chemotaxis: diacetyl (attractant)	ok	ok	ok
Chemotaxis: SDS (repellent) adults	**X**	ok	**X***
Chemotaxis: SDS (repellent) larvae	**X***	ok	**X**
Light touch assay	ok	ok	ND
Pharynx defects	**X**	ok	ok

ND: Not determined. OK indicates no alteration in phenotype with respect to the control. **X** indicates an altered phenotype with respect to the control. Asterisks indicate significant differences from control.

DISCUSSION

Here, we have shown that *C. elegans* NMGP-1 shares features with mammalian GPM6A and *D. melanogaster* M6. In COS-7 cells, NMGP-1 induced protrusion formation similarly to GPM6A and M6. Using two available *nmgp-1* mutants as well as RNAi-mediated *nmgp-1* knockdown, we have shown that *nmgp-1* is required for normal egg-laying and for timely exit of the dauer stage to resume the life cycle. In general, worms with *nmgp-1* deficiency that were grown under normal conditions behaved like worms exposed to unfavorable conditions, as demonstrated by reduced egg-laying and delayed recovery from the dauer stage. In addition, *nmgp-1* deficient worms exhibited ASJ chemosensory neurons with blebs and/or disrupted dendrites.

The evolution of the proteolipid protein family shows that *nmgp-1* is an ancestral gene of the PLP family present in *C. elegans* (Schweitzer *et al.* 2006). The alignments of NMGP-1 with *M. musculus* GPM6A and *D. melanogaster* M6 demonstrated a degree of conservation at the level of protein sequence. However, we found a noticeable difference in tertiary structure: Whereas GPM6A and M6 are comprised of four transmembrane domains, NMGP-1 contains only three. The single extracellular loop of NMGP-1 partially aligns with the major loop of M6 and GPM6A. In GPM6A, the major loop is required for filopodium outgrowth and synaptogenesis (Fuchsova *et al.* 2009). Moreover, four cysteine residues are required to form intramolecular disulfide bonds (Fuchsova *et al.* 2009) for the proper folding of this loop (Dhaunchak and Nave 2007). These cysteines are also present in the extracellular loop of NMGP-1, suggesting that the loop and, possibly, its function have been conserved. Several candidate sites for posttranslational modifications, especially in the C-terminus of NMGP-1, are also conserved. For example, sites in rat GPM6A that are phosphorylated by casein kinase 2 (CK2) and phosphokinase C (PKC) and are required for synaptogenesis (Brocco *et al.* 2010), as well as a tyrosine residue shown to be involved in neurite outgrowth (Formoso *et al.* 2015a) both have counterparts in NMGP-1. Finally, heterologous expression in COS-7 cells showed that, like GPM6A, NMGP-1 localized to the plasma membrane and induced filopodium formation. These results support the notion that NMGP-1 and GPM6A are functional orthologs.

To characterize the function of *nmgp-1* in *C. elegans,* we used two available *nmgp-1* mutant strains as well as *nmgp-1(RNAi)*-treated worms. The *nmgp-1(tm5483)* allele has a large deletion in the *nmgp-1* gene, so the MYM 001 mutant strain may express a truncated protein lacking its extracellular loop (Figure 1B, D). Due to the key functional role of this domain, the mutant protein is predicted to be nonfunctional. The *nmgp-1(gk144571)* allele in the MYM 002 strain has a methionine 39 to isoleucine mutation. This allele belongs to the Million Mutation Project (MMP). Although we have backcrossed the mutant strain according to standard

procedures, strains from MMP are heavily mutated and background mutations could still be present in the MYM 002 strain. However, rescue assays with the wild-type gene showing the recovery of pharynx morphology, egg-laying rate and bag-of-worm phenotype suggest that the mutation in *nmgp-1* is causative. Moreover, in vitro assays with the mutant protein mutNMGP-1 showed that the M39I mutation affects protein function. Bioinformatics analysis predicted that Met39 lies within the first transmembrane domain of NMGP-1 (conserved in the second transmembrane domain of *D. melanogaster* M6). Our *in vitro* studies showed that mutated NMGP-1 was unable to promote filopodium formation, indicating that methionine 39 is required for normal NMGP-1 function. This is consistent with previous work showing that two non-synonymous SNPs located in GPM6A transmembrane domain 2 (F93C and I97S) block filopodium induction in hippocampal neurons (Formoso *et al.* 2015b). Furthermore, GPM6A amino acids F93 and I97 (highlighted in Figure 1B) are located in the same region as M39 of NMGP-1, suggesting that this region within the transmembrane domain is key to protein function. Proteolipid proteins self-associate in the plasma membrane through transmembrane domains (Ng and Deber 2014; Formoso *et al.* 2015b), thus changes in those domains might alter homotypic interactions in mutant proteolipid proteins.

Due to the structural and functional similarities between GPM6A, M6 and NMGP-1 and because proteolipid proteins are expressed in neurons, we hypothesized that NMGP-1 was expressed in the nervous system of the worm. Two RNA-seq experiments (Hammarlund *et al.* 2019; Cao *et al.* 2017) revealed *nmgp-1* expression in neurons and glia at larval stages. Using a transcriptional reporter strain, we observed that neurons and glial cells were labelled in adult hermaphrodites. We then used strains with mutations in the *nmgp-1* gene as well as RNAi-mediated neuronal *nmgp-1* knockdown to study phenotypes that require neural input. We found several altered phenotypes, showing that worms require wild-type *nmgp-1* for normal nervous system functioning.

GPM6A has been shown to mediate responses to stress (Alfonso *et al.* 2004; Monteleone *et al.* 2014; Monteleone *et al.* 2017). To evaluate this function in worms, we used starvation to induce stress in *ngmp-1*-deficient worms. We observed that these worms failed to exit the dauer stage in the same time frame as controls, which can be interpreted as a defect in detecting the end of a stressful stage. Whole-animal RNA-sequencing of dauer and L4 (just after re-entering in life cycle) larvae showed that *nmgp-1* levels are greatly reduced in dauer larvae and highly increased in L4 (Lee *et al.* 2017). This may explain why mutants or *nmgp-1(RNAi*)-treated worms showed a slowdown in dauer recovery and resumption of the life cycle and highlights the need for *nmgp-1* to reenter the life cycle. The nervous system controls entry into and exit from the dauer

stage, particularly via the amphid sensory organ, which is composed of chemosensory neurons and associated glial sheath and socket cells (Bargmann and Horvitz 1991). Chemosensory neuron dendrites end in cilia, tiny specialized membrane structures that are exposed to the environment and detect ambient cues (White *et al.* 1986). Defects in cilium architecture have been associated with poor dauer recovery (Hu 2007). We have demonstrated that, *in vitro*, the protein NMGP-1 has the ability to induce the formation of membrane protrusions, thus we propose that, *in vivo*, the protein NMGP-1 may participate in cilium formation in cells of the sensory organ. By contrast, low *nmgp-1* levels may produce limited protein quantity altering the cilium architecture of some of those cells, including ASJ neurons, that mediates dauer exit (Chung *et al.* 2013) and this may explain the delayed dauer recovery observed in *nmgp-1(RNAi)*-treated worms. Accordingly, analysis of *nmgp-1* reporter expression showed labelling of many head neurons, including sensory ones. Moreover, the databases C. elegans Neuronal Gene Expression Map & Network (CeNGEN) (Hammarlund *et al.* 2019) and the Cell Atlas of Worm (Cao *et al.* 2017) show that *nmgp-1* is expressed in ASJ, ASK and PVD sensory neurons and also in I1, I2 and I3 pharyngeal interneurons, PVC ventral interneuron and MC pharyngeal motor neurons (see Supplementary Tables 1 and 2). All these neurons have been postulated as sensory neurons (Albertson and Thomson 1976). This suggests that additional sensory neurons expressing *nmgp-1* may be compromised in *nmgp-1* mutant or *nmgp-1(RNAi)*-treated worms.

We found a reduction in the serotonin-induced egg-laying rate in *nmgp-1* mutant alleles or *nmgp-1(RNAi)* worms compared to controls. This suggests that lack of *nmgp-1* impairs the normal function of cells within the egg-laying apparatus. Downstream of HSN cells are VC neurons and vulval muscle cells. VC neurons innervate vulval muscles and drive egg-laying. Results from our levamisole assays suggest that vulval muscles function properly in *nmgp-1* mutants. We propose that *nmgp-1* mutations could affect egg-laying through defects in VC neurons. In addition, VC neurons are stimulated by HSN neurons, which are postsynaptic to ASJ neurons (*C. elegans* Neural Network (Chen *et al.* 2006)). Since environmental detection mediated by sensory neurons contributes to egg-laying (Schafer 2006; Trent *et al.* 1983), we suggest that the observed egg-laying failure in *nmgp-1* mutants and in *nmgp-1(RNAi)*-treated worms may be, in part, due to defects in sensory neurons, such as those observed in ASJ. Alternatively, failure in egg-laying may be related to altered function of other *nmgp-1* expressing cells within the egg-laying apparatus.

In addition to morphological defects shown in the ASJ neurons, we propose that *nmgp-1* deficiency may affect other sensory neurons. *nmgp-1* mutations did not disturb the chemotactic behavior of diacetyl

attraction, which is mediated mainly by AWA and AWB neurons (Sengupta *et al.* 1996), indicating that these cells may remain intact in mutant or *nmgp-1(RNAi)*-treated worms. However, the avoidance response to SDS was impaired in *nmgp-1* mutants, suggesting that neurons involved in avoidance such as ASH neurons may also be affected. Escape behavior involves the coordination of head (amphid) and tail (phasmid) sensory neurons (Hilliard *et al.* 2002), and phasmid neurons modulate chemorepulsion behavior. We found that *nmgp-1* was expressed in head and tail sensory neurons, which might explain the altered response of *nmgp-1* mutants in avoidance assays.

Morphological changes observed in pharynges may be related to *nmgp-1* expression in some pharynx cells as reported in the CeNGEN database (Hammarlund *et al.* 2019, Supplementary Table 1) and observed in NeuroPAL strain injected with *Pnmgp-1::GFP*. Defects in the pharynx of *nmgp-1* mutants resemble the twisted pharynx reported by Axäng et al. (2007). These authors report that this phenotype can be caused at larval stages by defects in proteins involved in extracellular adhesion or in cytoskeleton regulation (Axäng *et al.* 2007). These functions have also been attributed to GPM6A (Fuchsova *et al.* 2009; Alfonso *et al.* 2005). Furthermore, as mentioned, vertebrates express several PLP proteins in different cell types, including glial cells. In worms, NMGP-1 is the only PLP protein, so it is likely that it fulfills the PLP function in all cell types. Therefore, or in addition to the observed neuronal defects, worms with mutations in the *nmgp-1* gene could also have impaired glial cells. In *C. elegans*, all glial cells are associated with sensory organs. The amphid sensory organ consists of 12 sensory neurons, including ASJ and ASH neurons and the sheath and socket glial cells. Glial cells form openings through which cilia from chemosensory neurons (White *et al.* 1986) are exposed to the environment. *nmgp-1* appeared to be expressed in CEPsh cells. The CeNGEN database (Hammarlund *et al.* 2019) indicates that *nmgp-1* is expressed in amphid sheath cells (see Supplementary Table 1). Therefore, the phenotypes exhibited by *nmgp-1* mutant worms might also be a consequence of damaged glial cells that would prevent the proper functioning of sensory neurons.

nmgp-1 deficiency affected egg-laying, dauer recovery and sensing of some environmental cues. PLP proteins from other organisms may share these features. For example, *D. melanogaster* M6 mutants exhibit a defective response to light (Zappia *et al.* 2012) and GPM6A mutant mice exposed to mild stress develop claustrophobia-like behavior (El-Kordi *et al.* 2013). Adverse environments or misperception affect organism homeostasis and induce a stress state. In the mammalian brain, chronic stress modulates mRNA expression of *nmgp-1* orthologs, such as *Gpm6a, Gpm6b and Dm20* (Alfonso *et al.* 2004; Fernández *et al.* 2010). Thus, PLP

proteolipid proteins might participate in an ancient response to stressful environments. Recently, Dwyer has proposed that conserved genes sustain essential behaviors crucial for survival (e.g., stress coping) and that evolution only refines those behaviors (Dwyer 2017). This might be true for genes implicated in psychiatric illness (Dwyer 2017). Some neuropsychiatric diseases, such as depression, have been shown to alter *GPM6A* mRNA levels (Fuchsova *et al.* 2015), and *GPM6A* gene polymorphisms have been associated with neuropsychiatric pathologies (Boks *et al.* 2008; Greenwood *et al.* 2012; El-Kordi *et al.* 2013). Chronic stress constitutes a preponderant risk factor for these pathologies; thus, stress studies will contribute to understanding mood disorders. Intriguingly, mood diseases are treated with antipsychotic drugs that have also been shown to reduce dauer recovery (Weeks *et al.* 2010), the same behavior that we have shown to be disturbed in worms with *nmgp-1* deficiency. Hence, we propose *nmgp-1* mutant worms as a powerful model to shed light into the mechanisms underlying the stress response and related diseases such as neuropsychiatric illnesses.

CONFLICT-OF-INTEREST AND FINANCIAL DISCLOSURE STATEMENT

The authors declare no biomedical financial interest or potential conflicts of interest.

--Human subjects --
Involves human subjects:
If yes: Informed consent & ethics approval achieved:
=> if yes, please ensure that the info "Informed consent was achieved for all subjects, and the experiments were approved by the local ethics committee." is included in the Methods.
ARRIVE guidelines have been followed:
Yes
=> if it is a Review or Editorial, skip complete sentence => if No, include a statement in the "Conflict of interest disclosure" section: "ARRIVE guidelines were not followed for the following reason:
"
(edit phrasing to form a complete sentence as necessary).
=> if Yes, insert in the "Conflict of interest disclosure" section:
"All experiments were conducted in compliance with the ARRIVE guidelines." unless it is a Review or Editorial

Conflicts of interest: None

=> if 'none', insert "The authors have no conflict of interest to declare."

=> else insert info unless it is already included

Open Science Badges

No, I am not interested to achieve Open Science Badge(s) => if yes, please see Comments from the Journal for further information => if no, no information needs to be included in the manuscript.

ACKNOWLEDGEMENTS

The authors thank the Caenorhabditis Genetics Center, funded by NIH Office of Research Infrastructure Programs (P40 OD010440) for N2 stock. We also thank the International *C. elegans* Gene Knockout Consortium (*C. elegans* Gene Knockout Facility at the Oklahoma Medical Research Foundation, funded by the NIH) and the *C. elegans* Reverse Genetics Core Facility (at the University of British Columbia, funded by the Canadian Institute for Health Research, Genome Canada, Genome BC, the Michael Smith Foundation, and the National Institutes of Health) for the VC20170 (allele *gk144571*), TU3595 and OE3010 strains. Finally, we thank the National BioResource Project, Tokyo, Japan for providing the *tm5483* knockout stock. We thank Silvia Billi Ph.D. and Vanina Campo Ph.D. for critical reading of the manuscript. EMF is a fellow of the Consejo Nacional de Investigaciones Científicas y Técnicas of Argentina (CONICET). MCM and MAB are researchers from CONICET. Funding: This work was supported by the National Agency for Scientific and Technological Promotion (ANPCyT, PICT-2017-1736 and PICT-2016-01710 to MAB and ACF).

All strains generated for this study are available upon reasonable request.

REFERENCES

Albertson D. G., Thomson J. (1976) The pharynx of Caenorhabditis elegans. *Philos Trans R Soc L. B Biol Sci.* **275**, 299–325.

Alfonso J., Fernández M. E., Cooper B., Flugge G., Frasch A. C. (2005) The stress-regulated protein M6a is a key modulator for neurite outgrowth and filopodium/spine formation. *Proc. Natl. Acad. Sci. U. S. A.* **102**, 17196–201.

Alfonso J., Frick L. R., Silberman D. M., Palumbo M. L., Genaro A. M., Frasch A. C. (2006) Regulation of hippocampal gene expression is conserved in two species subjected to different stressors and antidepressant treatments. *Biol. Psychiatry* **59**, 244–51.

Alfonso J., Pollevick G. D., Hart M. G. van der, Flugge G., Fuchs E., Frasch A. C. C. (2004) Identification of genes regulated by chronic psychosocial stress and antidepressant treatment in the hippocampus. *Eur. J. Neurosci.* **19**, 659–666.

Axäng C., Rauthan M., Hall D. H., Pilon M. (2007) The twisted pharynx phenotype in C. elegans. *BMC Dev. Biol.* **7**, 1–13.

Bargmann C. I., Hartwieg E., Horvitz H. R. (1993) Odorant-selective genes and neurons mediate olfaction in C. elegans. *Cell* **74**, 515–527.

Bargmann C. I., Horvitz H. R. (1991) Control of larval development by chemosensory neurons in Caenorhabditis elegans. *Science* **251**, 1243–6.

Baumeister R. (2002) The worm in us – Caenorhabditis elegans as a model of human disease. *TRENDS in Biotec hnology* **20**, 147–148.

Belmonte M. K., Jr E. H. C., Anderson G. M., Rubenstein J. L. R., Greenough W. T. (2004) Autism as a disorder of neural information processing: directions for research and targets for therapy 1. *Mol. Psychiatry* **9**, 646–663.

Bhattacharya A., Aghayeva U., Berghoff E.G., Hobert O. Plasticity of the Electrical Connectome of C. elegans (2019), *Cell* 176, 1174–1189.

Boks M. P. M., Hoogendoorn M., Jungerius B. J., Bakker S. C., Sommer I. E., Sinke R. J., Ophoff R. A., Kahn R. S. (2008) Do mood symptoms subdivide the schizophrenia phenotype? Association of the GMP6A gene with a depression subgroup. *Am. J. Med. Genet. B. Neuropsychiatr. Genet.* **147B**, 707–11.

Brenner S. (1974) The genetics of Caenorhabditis elegans. *Genetics* **77**, 71–94.

Brewer J. C., Olson A. C., Collins K. M., Koelle M. R. (2019) Serotonin and neuropeptides are both released by

the HSN command neuron to initiate C. elegans egg laying. *PLoS Genet.* **15**, 1–26.

Brocco M. A., Fernández M. E., Frasch A. C. C. (2010) Filopodial protrusions induced by glycoprotein M6a exhibit high motility and aids synapse formation. *Eur. J. Neurosci.* **31**, 195–202.

Bromberg Y., Yachdav G., Rost B. (2008) SNAP predicts effect of mutations on protein function. *Bioinformatics* **24**, 2397–8.

Calahorro F., Ruiz-Rubio M. (2011). Caenorhabditis elegans as an experimental tool for the study of complex neurological diseases: Parkinson's disease, Alzheimer's disease and autism spectrum disorder. *Invert Neurosci* **11**:73–83

Received:

Calixto A., Chelur D., Topalidou I., Chen X. (2011) Enhanced neuronal RNAi in C. elegans using SID-1. *Nat Methods.* **7**, 554–559.

Cao J., Packer J. S., Ramani V., Cusanovich D. A., Huynh C., Daza R., Qiu X., et al. (2017) Comprehensive single cell transcriptional profiling of a multicellular organism. *Science.* **357**, 661–667.

Carnell L., Illi J., Hong S. W., McIntire S. L. (2005) The G-protein-coupled serotonin receptor SER-1 regulates egg laying and male mating behaviors in Caenorhabditis elegans. *J. Neurosci.* **25**, 10671–81.

Chen B. L., Hall D. H., Chklovskii D. B. (2006) Wiring optimization can relate neuronal structure and function. *Proc. Natl. Acad. Sci. U. S. A.* **103**, 4723–4728.

Chung S. H., Schmalz A., Ruiz R. C. H., Gabel C. V, Mazur E. (2013) Femtosecond laser ablation reveals antagonistic sensory and neuroendocrine signaling that underlie C. elegans behavior and development.Chung SH, Schmalz A, Ruiz RCH, Gabel C V, Mazur E (2013) Femtosecond laser ablation reveals antagonistic sensory and neu. *Cell Rep.* **4**, 316–26.

Dhaunchak A.-S., Nave K.-A. (2007) A common mechanism of PLP/DM20 misfolding causes cysteine-mediated endoplasmic reticulum retention in oligodendrocytes and Pelizaeus-Merzbacher disease. *Proc. Natl. Acad. Sci. U. S. A.* **104**, 17813–8.

Dwyer D. S. (2017) Crossing the Worm-Brain Barrier by Using Caenorhabditis elegans to Explore Fundamentals of Human Psychiatric Illness. *Mol. Neuropsychiatry* **3**, 170–179.

El-Kordi A., Kästner A., Grube S., Klugmann M., Begemann M., Sperling S., Hammerschmidt K., et al. (2013) A

single gene defect causing claustrophobia. *Transl. Psychiatry* **3**, 1–12.

Fernández M. E., Alfonso J., Brocco M. A., Frasch A. C. (2010) Conserved cellular function and stress-mediated regulation among members of the proteolipid protein family. *J. Neurosci. Res.* **88**, 1298–308.

Formoso K., Billi S. C., Frasch A. C., Scorticati C. (2015a) Tyrosine 251 at the C-terminus of neuronal glycoprotein M6a is critical for neurite outgrowth. *J. Neurosci. Res.* **93**, 215–29.

Formoso K., García M. D., Frasch A. C., Scorticati C. (2015b) Filopodia Formation driven by Membrane Glycoprotein M6a depends on the Interaction of its Transmembrane Domains. *J. Neurochem.* **134**, 499–512.

Fuchsova B., Alvarez-Juliá A., Rizavi H. S., Frasch A. C., Pandey G. N. (2015) Altered expression of neuroplasticity-related genes in the brain of depressed suicides. *Neuroscience* **299**, 1–17.

Fuchsova B., Fernández M. E., Alfonso J., Frasch A. C. (2009) Cysteine residues in the large extracellular loop (EC2) are essential for the function of the stress-regulated glycoprotein M6a. *J. Biol. Chem.* **284**, 32075–88.

Ghosh D. D., Nitabach M. N., Zhang Y., Harris G. (2017) Multisensory integration in C. elegans. *Curr. Opin. Neurobiol.* **43**, 110–118.

Greenwood T. a, Akiskal H. S., Akiskal K. K., Kelsoe J. R. (2012) Genome-wide association study of temperament in bipolar disorder reveals significant associations with three novel Loci. *Biol. Psychiatry* **72**, 303–10.

Hammarlund M., Hobert O., Miller D. M., Sestan N. (2019) The CeNGEN Project: The Complete Gene Expression Map of an Entire Nervous System. *Neuron* **99**, 430–433.

Hardaker L. A., Singer E., Kerr R., Zhou G., Schafer W. R. (2001) Serotonin modulates locomotory behavior and coordinates egg-laying and movement in Caenorhabditis elegans. *J. Neurobiol.* **49**, 303–13.

Hilliard M. A., Bargmann C. I., Bazzicalupo P. (2002) C. elegans responds to chemical repellents by integrating sensory inputs from the head and the tail. *Curr. Biol.* **12**, 730–734.

Hobert O. (2002) PCR fusion-based approach to create reporter Gene constructs for expression analysis in transgenic C. elegans. *Biotechniques* **32**, 728–730.

Hsieh Y. W., Alqadah A., Chuang C. F. (2017) Mechanisms controlling diversification of olfactory sensory

neuron classes. *Cell. Mol. Life Sci.* **74**, 3263–3274.

Hughes K. J., Rodriguez A., Flattb K. M., Rayc S., Schuler A., Rodemoyer B., Veerappan V., Cuciarone K., Kullman A., Lim C., Gutta N., Vemuri S., Andriulis V., Niswonger D., Barickman L., Stein W., Singhvi W., Schroeder N. E., Vidal-Gadea A. G. (201) Physical exertion exacerbates decline in the musculature of an animal model of Duchenne muscular dystrophy. *Proc. Natl. Acad. Sci. U. S. A.* **116**, 3508–3517.

Hu P. J. (2007) Dauer. *WormBook*, 1–19.

Iliff A.J., Shawn Xu X.Z. (2020) C. elegans: a sensible model for sensory biology, *J Neurogenetics*, DOI: 10.1080/01677063.2020.1823386

Karp, X. Working with dauer larvae. (August 9, 2018), WormBook, ed. The C. elegans Research Community, WormBook, doi/10.1895/ wormbook.1.180.1, http://www.wormbook.org.

Kim J., Poole D. S., Waggoner L. E., Kempf A., Ramirez D. S., Treschow P. A., Schafer W. R. (2001) Genes affecting the activity of nicotinic receptors involved in Caenorhabditis elegans egg-laying behavior. *Genetics* **157**, 1599–1610.

Kim W., Underwood R. S., Greenwald I., Shaye D. D. (2018) Ortholist 2: A new comparative genomic analysis of human and caenorhabditis elegans genes. *Genetics* **210**, 445–461.

Krogh A., Larsson B., Heijne G. Von, Sonnhammer E. L. L. (2001) Predicting transmembrane protein topology with a hidden Markov model: Application to complete genomes. *J. Mol. Biol.* **305**, 567–580.

Lagenaur C., Kunemund V., Fischer G., Fushiki S., Schachner M. (1992) Monoclonal M6 antibody interferes with neurite extension of cultured neurons. *J. Neurobiol.* **23**, 71–88.

Lai C. H., Chou C. Y., Ch'ang L. Y., Liu C. S., Lin W. C. (2000) Identification of novel human genes evolutionarily conserved in Caenorhabditis elegans by comparative proteomics. Genome Res. 10, 703–713.

Lee J. S., Shih P.-Y., Schaedel O. N., Quintero-Cadena P., Rogers A. K., Sternberg P. W. (2017) FMRFamide-like peptides expand the behavioral repertoire of a densely connected nervous system. *Proc. Natl. Acad. Sci.* **114**, E10726–E10735.

Matsuura T., Izumi J., Hioki M., Nagaya H., Kobayashi Y. (2013) Sensory Interaction Between Attractant Diacetyl and Repellent 2-Nonanone in the Nematode Caenorhabditis elegans. *J. Exp. Zool. Part A Ecol. Genet. Physiol.* **319**, 285–295.

Michibata H., Okuno T., Konishi N., Wakimoto K., Kyono K., Aoki K., Kondo Y., Takata K., Kitamura Y., Taniguchi T. (2008) Inhibition of mouse GPM6A expression leads to decreased differentiation of neurons derived from mouse embryonic stem cells. *Stem Cells Dev.* **17**, 641–51.

Monteleone M., Adrover E., Pallarés M., Antonelli M. C., Frasch A. C., Brocco M. A. (2014) Prenatal stress changes the glycoprotein GPM6A gene expression and induces epigenetic changes in rat offspring brain. *Epigenetics* **9**, 152–60.

Monteleone M. C., Billi S. C., Brocco M. A., Frasch A. C. (2017) Neural glycoprotein M6a is released in extracellular vesicles and modulated by chronic stressors in blood. *Sci. Rep.* **7**, 1–12.

Mukobata S., Hibino T., Sugiyama A., Urano Y., Inatomi A., Kanai Y., Endo H., Tashiro F. (2002) M6a acts as a nerve growth factor-gated Ca2+ channel in neuronal differentiation. *Biochem. Biophys. Res. Commun.* **297**, 722–728.

Nestler E. J., Barrot M., DiLeone R. J., Eisch A. J., Gold S. J., Monteggia L. M. (2002) Neurobiology of Depression. *Neuron* **34**, 13–25.

Ng D. P., Deber C. M. (2014) Terminal residue hydrophobicity modulates transmembrane helix-helix interactions. *Biochemistry* **53**, 3747–57.

Petersen B., Petersen T. N., Andersen P., Nielsen M., Lundegaard C. (2009) A generic method for assignment of reliability scores applied to solvent accessibility predictions. *BMC Struct. Biol.* **9**, 51.

Pigliucci M., Murren, C.J., Schlichting C.D. (2006) Phenotypic plasticity and evolution by genetic assimilation. The Journal of Experimental Biology 209, 2362-2367.

Porta-de-la-Riva M., Fontrodona L., Villanueva A., Cerón J. (2012) Basic Caenorhabditis elegans Methods: Synchronization and Observation. J. Vis. Exp. (64), e4019 10.3791/4019, DOI: 10.3791/4019.

Rost B., Yachdav G., Liu J. (2004) The PredictProtein server. *Nucleic Acids Res.* **32**, W321-6.

Schafer W. R. (2006) Genetics of Egg-Laying in Worms. *Annu. Rev. Genet.* **40**, 487–509.

Schweitzer J., Becker T., Schachner M., Nave K.-A., Werner H. (2006) Evolution of myelin proteolipid proteins: gene duplication in teleosts and expression pattern divergence. *Mol. Cell. Neurosci.* **31**, 161–77.

Sengupta P., Chou J. H., Bargmann C. I. (1996) Odr-10 Encodes a Seven-Transmembrane-Domain Olfactory Receptor Required for Responses to the Odorant Diacetyl. *Cell* **84**, 875–887.

Shaye D. D., Greenwald I. (2011) Ortholist: A compendium of C. elegans genes with human orthologs. *PLoS One* **6**.

Shtonda B. B., Avery L. (2006) Dietary choice behavior in Caenorhabditis elegans. *J Exp Biol. 2006* **209**, 89–102.

Stauffer T. P., Ahn S., Meyer T. (1998) Receptor-induced transient reduction in plasma membrane PtdIns(4,5)P2 concentration monitored in living cells. *Curr. Biol.* **8**, 343–6.

Stecca B., Southwood C. M., Gragerov A., Kelley K. A., Jr V. L. F., Gow A. (2000) The Evolution of Lipophilin Genes from Invertebrates to Tetrapods : DM-20 Cannot Replace Proteolipid Protein in CNS Myelin. *J. Neurosci.* **20**, 4002–4010.

Thierry-Mieg D., Thierry-Mieg J. (2006) AceView: a comprehensive cDNA-supported gene and transcripts annotation. *Genome Biol.* **7 Suppl 1**, S12.1-14.

Trent C., Tsuing N., Horvitz H. R. (1983) Egg-laying defective mutants of the nematode Caenorhabditis elegans. *Genetics* **104**, 619–647.

Urrutia A., García-Angulo V. A., Fuentes A., Caneo M., Legüe M., Urquiza S., Delgado S. E., Ugalde J., Burdisso P., Calixto A. (2020) *Bacterially produced metabolites protect C. elegans neurons from degeneration*.

Weeks K. R., Dwyer D. S., Aamodt E. J. (2010) Antipsychotic drugs activate the C. elegans akt pathway via the DAF-2 insulin/IGF-1 receptor. *ACS Chem. Neurosci.* **1**, 463–73.

White J. G., Southgate E., Thomson J. N., Brenner S. (1986) The Structure of the Nervous System of the Nematode Caenorhabditis elegans. *Philos. Trans. R. Soc. London. Ser. B, Biol. Sci.* **314**, 1–340.

Yan Y., Narayanan V., Lagenaur C. (1996) Expression of members of the proteolipid protein gene family in the developing murine central nervous system. *J. Comp. Neurol.* **370**, 465–78.

Yemini E., Albert Lin A., Nejatbakhsh A., Varol E., Sun R., Mena G.E., Samuel A.D.T., Paninski L., Venkatachalam V. Hobert O. (2021) NeuroPAL: A Multicolor Atlas for Whole-Brain Neuronal Identification in C. elegans *Cell* **184**, 272–288

Youngman M. J., Rogers Z. N., Kim D. H. (2011) A decline in p38 MAPK signaling underlies immunosenescence in Caenorhabditis elegans. *PLoS Genet.* **7**, e1002082.

Zappia M. P., Brocco M. A., Billi S. C., Frasch A. C., Ceriani M. F. (2011) M6 membrane protein plays an essential role in Drosophila oogenesis. *PLoS One* **6**, e19715.

Zappia M. P. M. P., Bernabo G., Billi S. C., Frasch A. C., Ceriani M. F. M. F., Brocco M. A. (2012) A role for the membrane protein M6 in the Drosophila visual system. *BMC Neurosci.* **13**, 78.

Zhao J., Iida A., Ouchi Y., Satoh S., Watanabe S. (2008) M6a is expressed in the murine neural retina and regulates neurite extension. *Mol. Vis.* **14**, 1623–30.

AUTHOR CONTRIBUTIONS

E.M.F carried out backcrosses, RNAi, behavioral tests, microscopy and image and data analysis. Y.B.C. carried out bioinformatics analysis, molecular cloning, cellular analysis and all initial worm backcrosses and behavioral tests. M.C.M. performed molecular cloning and cellular analysis. J.A. carried out microinjection assays. K.H. analyzed phenotypes after rescue and maintained stocks. J.A. and K.H. edited the manuscript. A.V.G. planned microinjection assays for mutant rescue and for neuron identification with NeuroPAL strain and wrote the manuscript. A.C.F. contributed reagents/materials. M.A.B. conceived and designed all the experiments and wrote the manuscript.

LEGENDS TO FIGURES

Figure 1. NMGP-1 tertiary structure is predicted to be similar to M6 and GPM6A. A) *nmgp-1* gene schema. Diagram (not scaled) shows exons and introns represented by boxes and lines, respectively. Black boxes represent untranslated regions (UTR) and white boxes highlight coding regions. The large grey box indicates the deleted region in the strain MYM 001 [*nmgp-1(tm5483)*] and the arrowhead indicates the methionine residue mutated in the strain MYM 002 [*nmgp-1(gk144571)*]. **B) NMGP-1 aligns with M6 and GPM6A.** BLASTp alignments between NMGP-1 and *D. melanogaster* M6 (isoform A) or *M. musculus* GPM6A are shown. In each alignment, the central line shows a consensus sequence, letters indicate conserved amino acids and a plus (+) symbol indicates similar amino acids. Gaps indicate a lack of similarity. NMGP-1 regions that align with transmembrane domains from *D. melanogaster* M6 are indicated by top square brackets. The grey box indicates the deleted region in NMGP-1 in the protein putatively expressed in strain MYM 001 [*nmgp-1(tm5483)*]. The black box indicates the mutated methionine residue in the strain MYM 002 [*nmgp-*

1(gk144571)]. Highlighted C and Y indicate cysteine residues in the extracellular loop and the tyrosine residue corresponding to Y251 from mouse GPM6A, respectively. Highlighted F and I are near methionine 39 and point out GPM6A non-synonymous SNPs that alter function (i.e., the ability to induce filopodia). **C) Protein topology of NMGP-1, *D. melanogaster* M6 and *M. musculus* GPM6A according to TMHMM predictions**. Graphs show the probability for the formation of transmembrane helices. Schemas on the top indicate extracellular regions (lines), transmembrane domains (boxes) and cytoplasmic regions (dashed lines). **D) Putative NMGP-1 structure.** The representation shows the three transmembrane domains, one extracellular loop (EC) and one intracellular loop (IC). Amino terminus (NH2) locates extracellularly and the carboxyl terminus (COOH) locates intracellularly. Symbols represent the sites for the putative posttranslational modifications (predicted using the PROSITE motif search) and the key cysteine residues that might maintain the extracellular loop structure along with the putative disulfide bridges (dashed lines). Arrowhead indicates the localization in the first transmembrane domain of the methionine residue mutated in the protein cloned from the MYM 002 [*nmgp-1(gk144571)*] strain (mutNMGP-1). The missing fragment in the putative truncated protein from the MYM 001 mutant is highlighted in grey.

Figure 2. Timeline of experimental procedures carried out. A. Worm synchronization. For lifespan assays, adults (P0) were allowed to lay eggs (F1) for 2 h. For the rest of the assays (see below), P0 worms were subjected to the hypochlorite bleaching method to obtain F1 eggs. Then, in both cases, eggs were transferred to a fresh plate and allowed growth to obtain adult F1 worms. N2 and mutant adult worms were assayed as F1. Worms from the RNAi-sensitive strain TU3595 were fed with HT115 bacteria (control or containing the plasmid to induce RNAi) from P0. To synchronize these worms, they were subjected to a second bleaching to obtain F2 eggs. **B. Assays.** Life span measurement was recorded from day 1 until all worms died; depending on genotype, worms survived between 15-21 days. *Anytime during lifespan analysis, worms with the bag-of-worm phenotype were excluded. On day 2, egg-laying, chemotaxis and morphological analysis were carried out. Dauer induction started on day 1. On day 10, F1-3 coexisted and dauer collection was done to measure dauer recovery time. Dauer larvae belonged to F2-4. **Worms that remained in origin (center of the plate) or in the quadrant boundaries and that were not anesthetized were excluded from the assay. ***Dauer larvae that did not move were registered as dead and were excluded from the assay. Numbers indicate the number of animals per experimental group (strain) and per replica and the number of excluded animals (if not indicated, no exclusion criteria were applied), between brackets.

Figure 3. NMGP-1 induces filopodium formation. COS-7 cells were transfected with plasmids to overexpress GFP, GPM6A-GFP, NMGP-1-GFP and mutNMGP-1-GFP. **A) Cells expressing the indicated recombinant proteins**. Left panel shows GFP expression. Right panel shows rhodamine-conjugated phalloidin to label F actin in the zoomed framed areas. Arrowheads point to GFP signal localized at the plasma membrane, black arrows point to filopodia and white arrows indicate GFP signal accumulated in the perinuclear zone. Scale bar, 10 µm. **B-C) Mutant NMGP-1 does not accumulate at the cell membrane but in the cytoplasm.** Confocal microscopy sections show cells transfected with NMGP-1-GFP or mutNMGP-1-GFP. White arrows indicate GFP signal accumulated in the perinuclear zone. (B). Using ImageJ software (plot profile tool), a line was drawn across the cell soma and the intensity from each pixel was obtained and plotted (C). **D) Quantification of the cells with filopodia.** Y-axis indicates the ratio between transfected filopodium-bearing cells versus non-transfected filopodium-bearing cells. Data are mean + SD. N = 40 to 45 cells per coverslip, 3 coverslips per condition in each of 3 independent cultures. One-way ANOVA followed by Tukey's multiple comparison tests for post hoc effects ($p<0.0001$).

Figure 4. *nmgp-1* reporter expresses in sensory neurons and in vulva cells. A 1.6kb promoter upstream of the *nmgp-1* start site was used to drive expression of GFP. **A) Head expression.** Image showing GFP expression in different head cell types, e.g., pharyngeal and amphid neurons and in particular large protein accumulation in regions consistent with the glial terminal processes. **B) Midbody expression.** In the medial region, we detected expression in the vulva. Cells labelled by *Pnmgp-1::GFP* could be CAN and HSN neurons (arrows). **C**) **Medial region expression.** Also in the medial region, *Pnmgp-1::GFP* labeled the dorsal cord (arrowheads). GFP expression in the egg (asterisk) indicates that *nmgp-1* expresses early in the development. **D) Tail expression.** *Pnmgp-1::GFP* also labelled some cells in the tail. We saw GFP expression in some phasmid neurons and probably in glial cells. Scale bar, 50 µm. **E-G) Images showing NeuroPAL (OH15550) strain injected with *Pnmgp-1::GFP.*** **E.** Image of the head of the worm showing the fluorescence of several fluorophores used as landmarks in the NeuroPAL strain (left). Specific combinations of colors allow identification of each neuron. On the right, *Pnmgp-1::GFP* signal is overlaid onto the left hand image. Worm's pharynx (**ph**), nerve ring (**nr**) and head ganglia (**hg**) show GFP expression, suggesting these cells normally express *nmgp-1*. **G.** Image of the worm's medial region expressing NeuroPAL fluorophores (left). Ventral cord is visible and individual cells can be identified. Overlapping (right) shows GFP expression under the *nmgp-1* promoter within the egg-laying apparatus. Arrows point to ventral cord cells expressing *nmgp-1.* Dotted line indicates slit, vulva (**vu**). **I.** Tail view of NeuroPAL strain (left). Overlapping of images from NeuroPAL

fluorophores and GFP expression under the *nmgp-1* promoter is shown on the right. Arrows point to tail ganglia and indicate *nmgp-1* expression.

Figure 5. Phenotypes of *nmgp-1* mutant strains and neuronal knockdown of *nmgp-1*. A) Mutant worms show an altered pharynx morphology. Images from control and both mutant strains show pharynges viewed with differential interference contrast (DIC) microscopy. The dotted lines outline the pharynx and highlight defects in the mutants. **B) Quantification of worms with a defective pharynx.** Bars represent the percentage of worms with pharynx defects. Nonparametric Kruskal–Wallis one-way ANOVA followed by Dunn's multiple comparison tests for *post hoc* effects ($p < 0.0001$ N2 vs. both alleles), n= 10-25 worms per strain in each of three independent plates. **C) Point mutation (Met39Ile) in *nmgp-1* gene reduces mean life span.** Percentage ± SE of N2, MYM 001 [*nmgp-1(tm5483)*] and MYM 002 [*nmgp-1(gk144571)*] living adult hermaphrodite worms versus time (days). Dashed line at 50 % indicates the mean lifespan, i.e., the time in which half of the population has died. N = 30 - 45 worms per strain in each of 3-5 independent plates. Log-Rank (Mantel-Cox) $p<0.1426$. Mean lifespan (i.e., the time in which half of the population has died) for MYM 002 [*nmgp-1(gk144571)*] was lower (7.2 ± 0.2 days vs. 9.3 ± 0.6 for N2 worms, Kruskal-Wallis statistics 6.331, n = 3-5 independent plates, $*p<0.03$). **D) *nmgp-1(RNAi)*-treated worms do not show an altered life span.** Percentage ± SE of control and *nmgp-1(RNAi)*-treated living adult hermaphrodite worms versus time (days). Dashed line at 50 % indicates worm half-life. Log-Rank (Mantel-Cox) $p<0.3502$), N = 45 - 55 worms per strain in each of 6-12 independent plates. **E) Mutant worms exhibit a subtly delayed recovery from dauer resistant stage.** Percentage ± SE of N2, MYM 001 [*nmgp-1(tm5483)*] and MYM 002 [*nmgp-1(gk144571)*] dauer larvae over time (hours). Dashed line at 50 % indicates mean dauer recovery time. Log-Rank (Mantel-Cox) $p<0.03$, n = 3 independent plates with 30 - 60 worms per strain. **F) *nmgp-1(RNAi)*-treated worms exhibit a delayed recovery from the dauer resistant stage.** Percentage ± SE of control and *nmgp-1(RNAi)*-treated dauer larvae over time (hours). Dashed line at 50 % indicates mean dauer recovery time. Log-Rank (Mantel-Cox) $***p<0.0001$, n=3 independent plates with 30 - 60 worms analyzed per strain.

Figure 6. *nmgp-1* is required for normal egg-laying. A) *nmgp-1 m*utant worms show reduced egg-laying. Bars represent the number of eggs laid by hermaphrodite worms after 1 h incubation in liquid medium M9 with (+) or without (-) 35 mM serotonin. Data are mean + SEM. One-way ANOVA $F(5,39) = 11.42$ with Brown-Forsythe post hoc test, n = 8 worms per strain in each of 5 independent plates, $p<0.0001$. **B) *nmgp-1(RNAi)* reduces egg-laying**. Bars represent the number of eggs laid by hermaphrodite worms after 1 h incubation in liquid

medium M9 with (+) or without (-) 35 mM serotonin. Data are mean + SEM. Non-parametric Kruskal–Wallis statistics followed by a Dunn's multiple comparison test for *post hoc* effects (**** p<0.001). n = 8 worms per strain in each of four independent plates. **C) Worms from both mutant strains show late embryos inside the uterus (bag-of-worms).** Images show the uterus of two N2 control hermaphrodites **(i)** and of MYM 001 [*nmgp-1(tm5483)*] **(ii)** and MYM 002 [*nmgp-1(gk144571)*] **(iii)** worms with embryos at stages usually observed outside the worm. Arrowheads indicate comma and pretzel stage embryos. **vu**, vulva. Scale bar is 50 µm. **D) Reduced egg-laying is accompanied by the bag-of-worm phenotype.** Images show the uterus of a **i)** control TU3595 hermaphrodite and of **ii-iii)** *nmgp-1(RNAi)*-treated worms with embryos at stages usually observed outside the worm (**ii**) and larvae (**iii**). Arrowheads indicate comma and pretzel stage embryos; arrows point out larvae. **vu**, vulva. **E) Quantification of the bag-of-worm phenotype.** Bars represent the percentage of worms containing embryos at stages usually observed outside the worm and/or larvae (classified as defective) or not (normal) for control and *nmgp-1(RNAi)*-treated worms. Data are mean + SEM. Nonparametric Kruskal–Wallis statistics followed by a Dunn's multiple comparison tests for *post hoc* effects (**p<0.005; N2 vs. MYM 001, n= 10-25 worms per strain in each of 10 independent plates. **F)** Quantification expressed as percentage of worms containing embryos at stages usually observed outside the worm and/or larvae (classified as defective) or not (normal) for control and *nmgp-1(RNAi)*-treated strains. Data are mean + SEM. **G) Egg-laying is restored in rescued *nmgp-1 m*utant worms**. Bars represent the number of eggs laid by hermaphrodite worms after 1 h incubation in liquid medium M9 with (+) or without (-) 35 mM serotonin. Data are mean + SEM. Kruskall-Wallis one-way ANOVA followed by Dunn's multiple comparison tests for *post hoc* effects, n = 8 worms per strain in each of 5-6 independent plates, p<0.18. **H) Mutants lay eggs when stimulated with levamisole in a dose response assay.** Bars represent the number of eggs per worm laid under increasing levamisole concentration. Levamisole concentration ranged from 0 to 50 µM. Data are mean + SEM. Two-way ANOVA, comparing main column effect, followed by Tukey's multiple comparisons test, interaction F = 0.8952, p>0.15, strain effect F = 3.498, p>0.18. n = 4 to 10 worms per strain in each concentration in each of 5 independent plates.

Figure 7. Chemosensation in worms with *nmgp-1* deficiency. A) ASJ neurons expressing GFP are morphologically altered. *nmgp-1(RNAi)*-treated worms from strain TU3595 x OE3010 were imaged with confocal microscopy. Arrows indicate dendrites and arrowheads point out blebs observed in the distal dendrite, near the sensilla opening. Scale bar is 10 µm. **B) Quantification of worms with defective neurons.**

Bars represent the percentage of worms with defects in ASJ neurons. Nonparametric Kruskal–Wallis statistics followed by a Dunn's multiple comparison tests for *post hoc* effects (*p<0.03), n= 10-25 worms per strain in each of 9 independent plates. **C, D) Attraction to diacetyl is not affected by *nmgp-1* mutations or knockdown.** Adult Worms (MYM 001 [*nmgp-1(tm5483)*] strain (**C**) and *nmgp-1(RNAi)*-treated (**D**)) were exposed to the attractant diacetyl and behavior recorded. No differences were observed between groups in the chemotaxis index. **E-I) Avoidance to SDS is lost in *nmgp-1* mutants and in *nmgp-1(RNAi)*-treated worms.** Worms were exposed to SDS and the avoidance index was calculated. MYM 001 [*nmgp-1(tm5483)*] strain (adults, **E** and larvae, **F**) and *nmgp-1(RNAi)*-treated worms (adults, **G**) did not avoid SDS and significantly differed from controls (p<0.03 for MYM 001 adults; p<0.02 for MYM 001 larvae; p<0.05 for *nmgp-1(RNAi)*). MYM 002 [*nmgp-1(gk144571)*] strain (adults and larvae, **E**, **F**) and *nmgp-1(RNAi)*-treated larvae (**H**) behaved like controls. **I**) Control non-treated worms classified as normal with respect to ASJ neuronal morphology and *nmgp-1(RNAi)*-treated worms classified as having defective ASJ neuron morphology were exposed to SDS and the avoidance index was calculated. Defective worms did not avoid SDS and significantly differed from controls (**p<0.007, n = 4-12 defective worms in each of 4 independent plates and n = 5-20 normal worms in each of 7 independent plates).

Figure 1

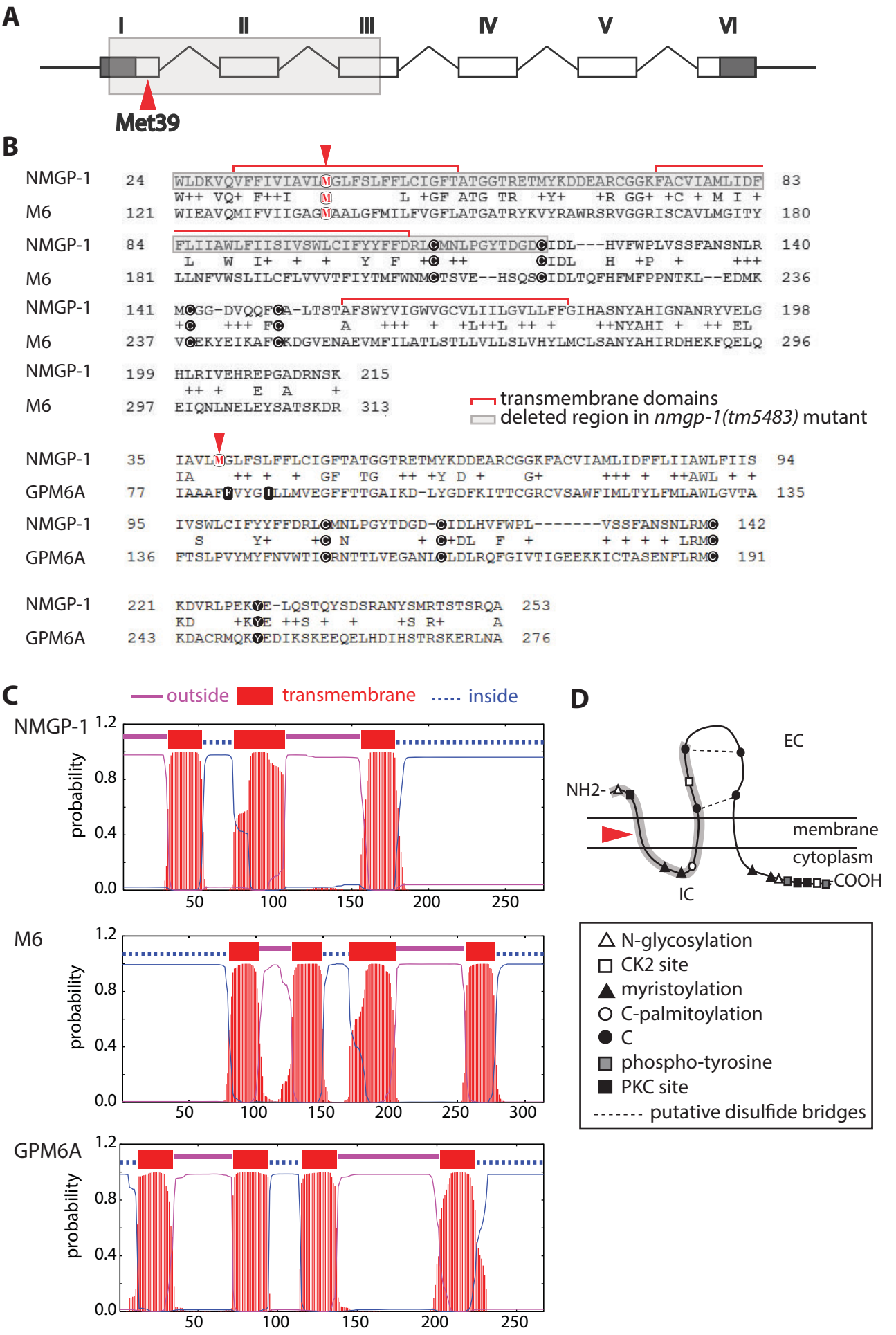
A
I
II
III
IV
V
VI
Met39
B
NMGP-1 24 WLDKVQVFFIVIAVLMGLFSLFFLCIGFTATGGTRETMYKDDEARCGGKFACVIAMLIDF 83
M6 121 WIEAVQMIFVIIGAGMAALGFMILFVGFLATGATRYKVYRAWRSRVGGRISCAVLMGITY 180
NMGP-1 84 FLIIAWLFIISIVSWLCIFYYFFDRLCMNLPGYTDGDCIDL---HVFWPLVSSFANSNLR 140
M6 181 LLNFVWSLILCFLVVVTFIYTMFWNMCTSVE--HSQSCIDLTQFHFMFPPNTKL--EDMK 236
NMGP-1 141 MCGG-DVQQFCA-LTSTAFSWYVIGWVGCVLIILGVLLFFGIHASNYAHIGNANRYVELG 198
M6 237 VCEKYEIKAFCKDGVENAEVMFILATLSTLLVLLSLVHYLMCLSANYAHIRDHEKFQELQ 296
NMGP-1 199 HLRIVEHREPGADRNSK 215
M6 297 EIQNLNELEYSATSKDR 313
transmembrane domains
deleted region in nmgp-1(tm5483) mutant
NMGP-1 35 IAVLMGLFSLFFLCIGFTATGGTRETMYKDDEARCGGKFACVIAMLIDFFLIIAWLFIIS 94
GPM6A 77 IAAAFRVYGILLMVEGFFTTGAIKD-LYGDFKITTCGRCVSAWFIMLTYLFMLAWLGVTA 135
NMGP-1 95 IVSWLCIFYYFFDRLCMNLPGYTDGD-CIDLHVFWPL-------VSSFANSNLRMC 142
GPM6A 136 FTSLPVYMYFNVWTICRNTTLVEGANLCLDLRQFGIVTIGEEKKICTASENFLRMC 191
NMGP-1 221 KDVRLPEKYE-LQSTQYSDSRANYSMRTSTSRQA 253
GPM6A 243 KDACRMQKYEDIKSKEEQELHDIHSTRSKERLNA 276
C
outside
transmembrane
inside
NMGP-1
M6
GPM6A
probability
0.0
0.4
0.8
1.2
50
100
150
200
250
300
D
EC
NH2-
membrane
cytoplasm
COOH
IC
N-glycosylation
CK2 site
myristoylation
C-palmitoylation
C
phospho-tyrosine
PKC site
putative disulfide bridges

Figure 2

A. Synchronization

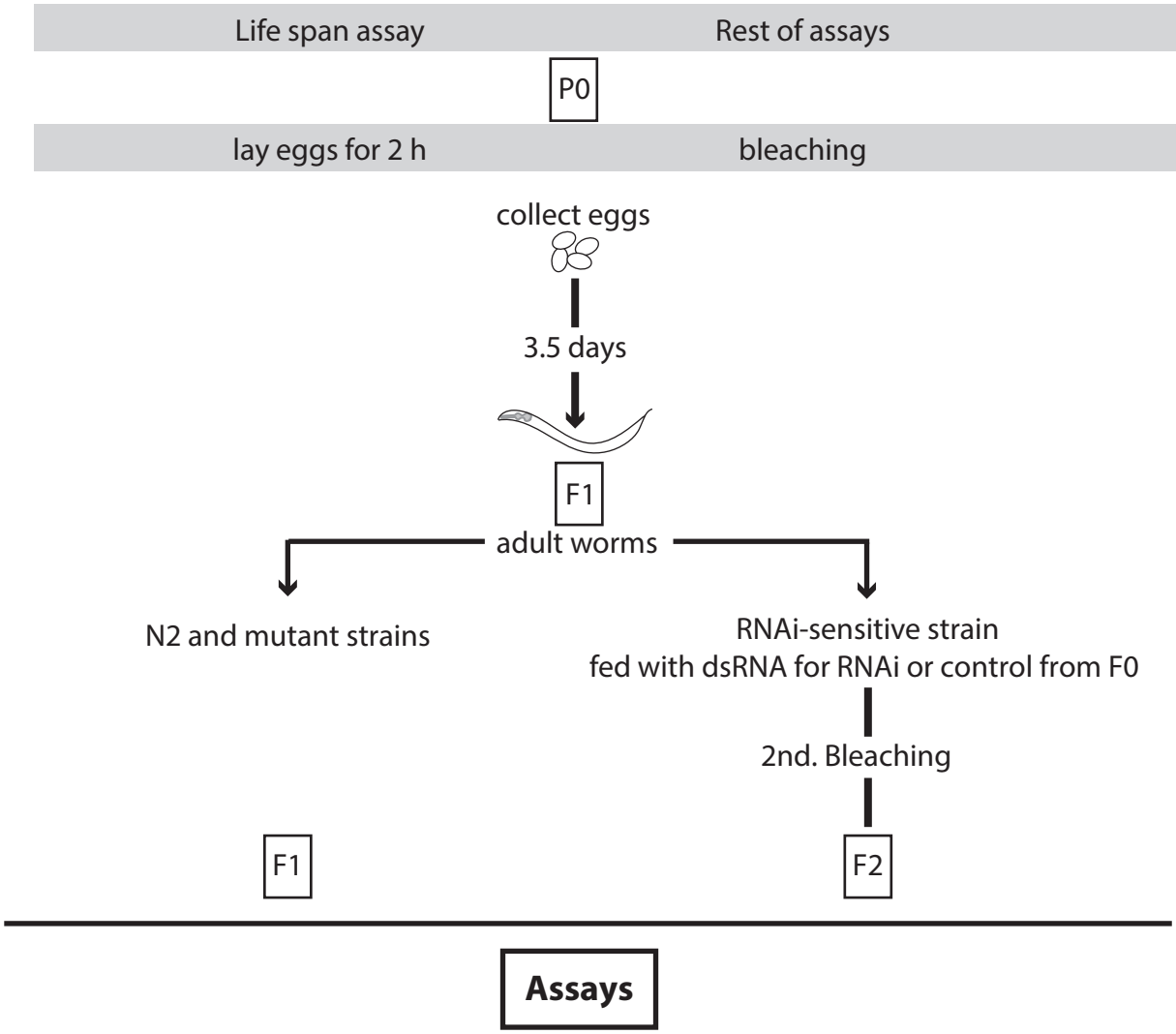

B. Assays

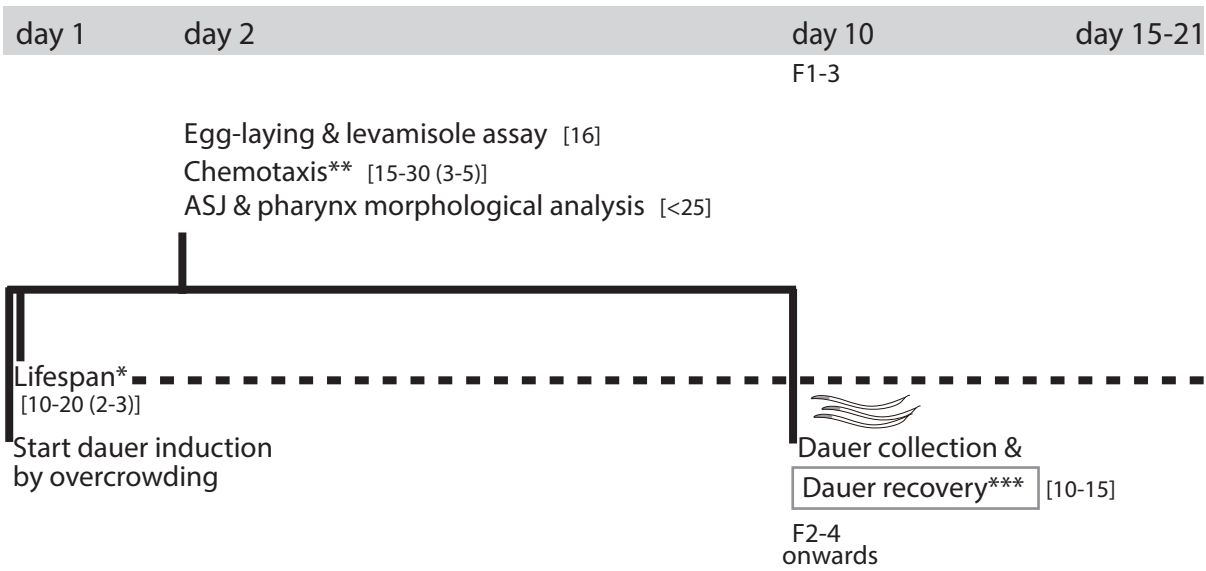

Figure 3

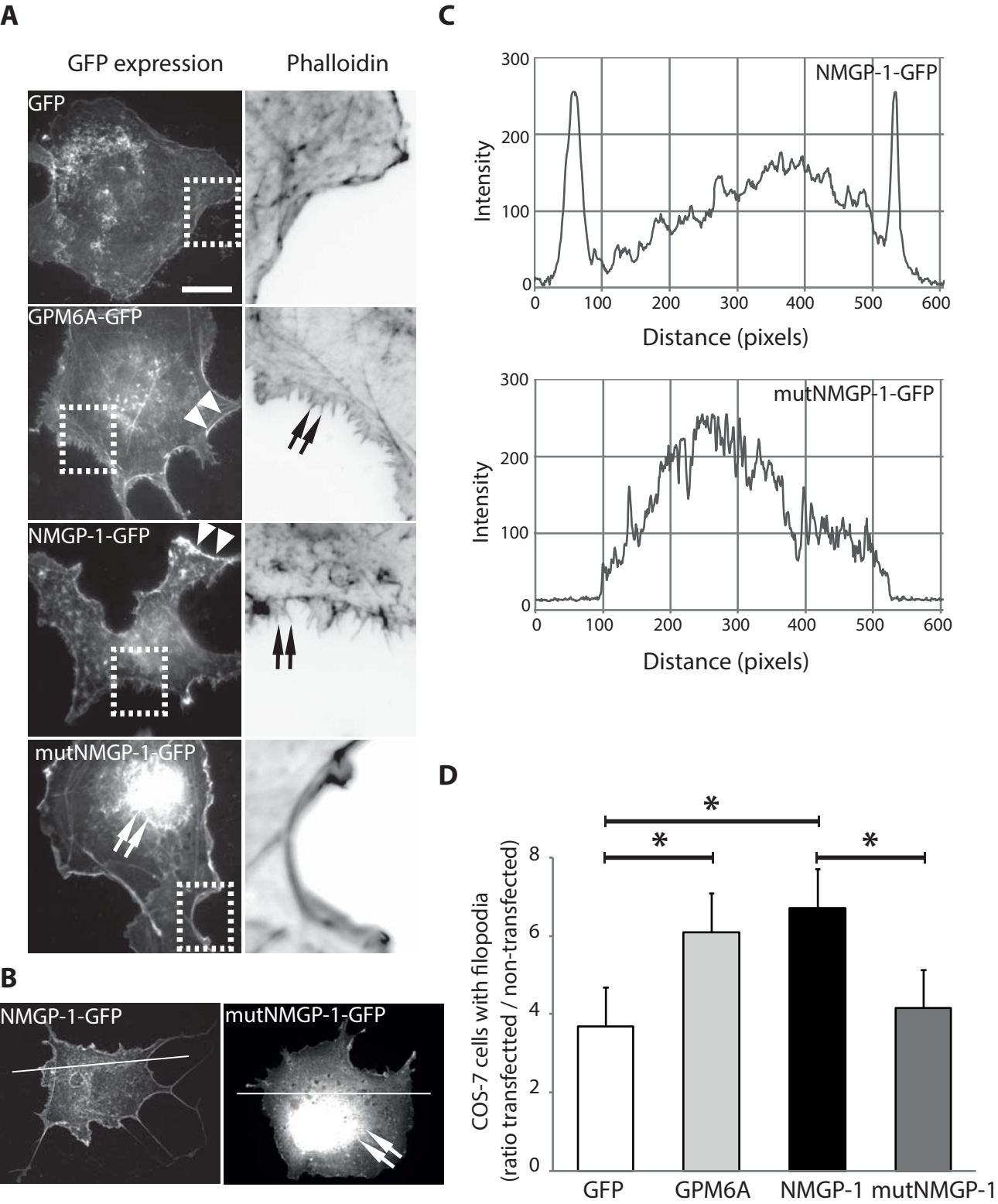
A
GFP expression
Phalloidin
GFP
GPM6A-GFP
NMGP-1-GFP
mutNMGP-1-GFP
B
NMGP-1-GFP
mutNMGP-1-GFP
C
NMGP-1-GFP
Intensity
Distance (pixels)
mutNMGP-1-GFP
Intensity
Distance (pixels)
D
COS-7 cells with filopodia
(ratio transfectted / non-transfected)
GFP
GPM6A
NMGP-1
mutNMGP-1

Figure 4

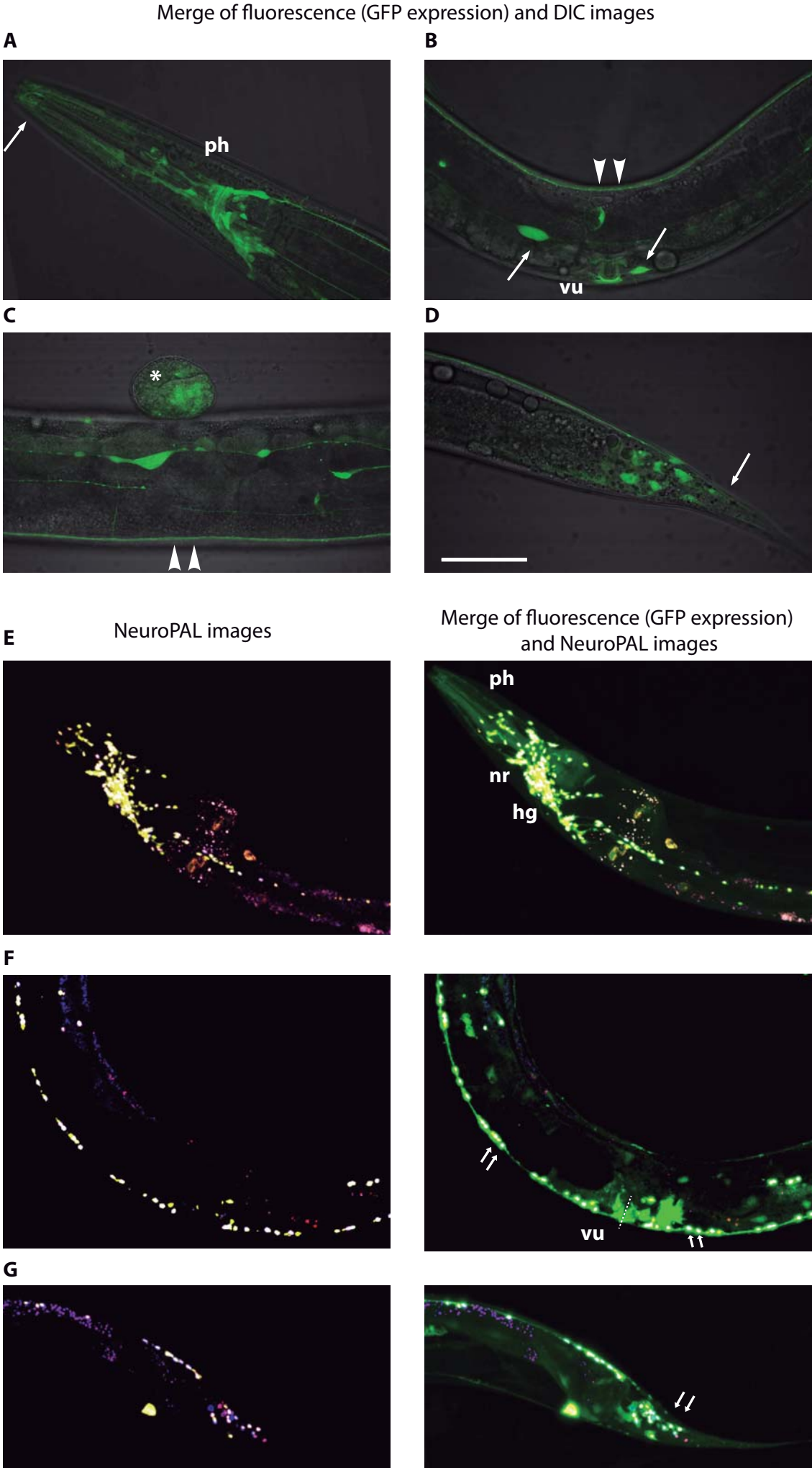
Merge of fluorescence (GFP expression) and DIC images
A
ph
B
vu
C
*
D
E
NeuroPAL images
Merge of fluorescence (GFP expression) and NeuroPAL images
ph
nr
hg
F
vu
G

Figure 4

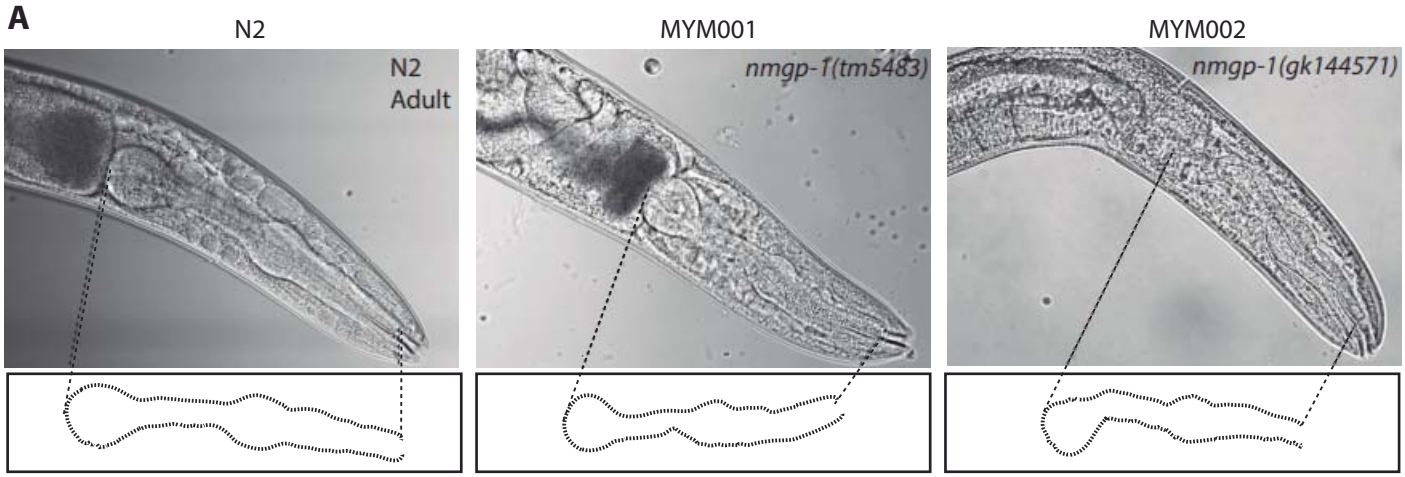
A
N2
MYM001
MYM002
N2
Adult
nmgp-1(tm5483)
nmgp-1(gk144571)

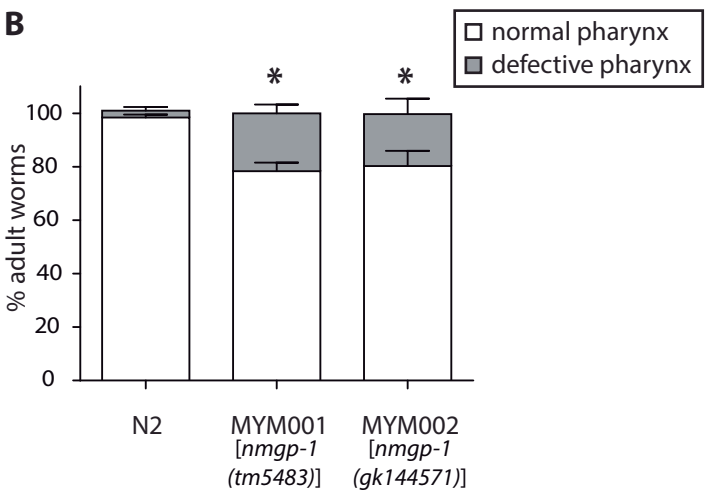
B
normal pharynx
defective pharynx
% adult worms
100
80
60
40
20
0
*
*
N2
MYM001 [nmgp-1 (tm5483)]
MYM002 [nmgp-1 (gk144571)]

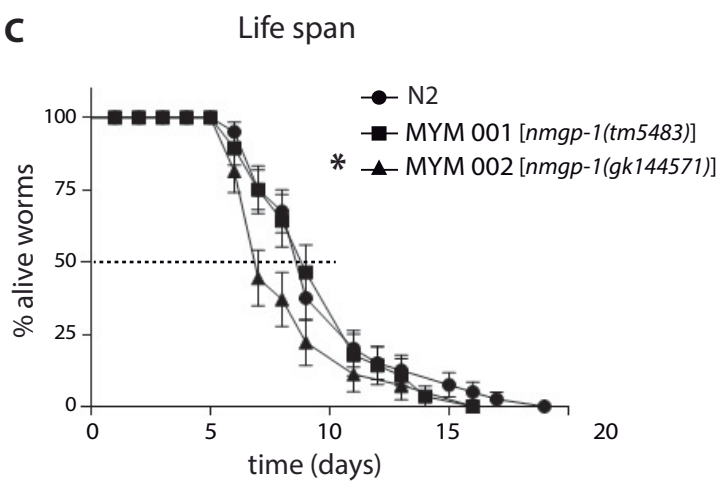
C
Life span
N2
MYM 001 [nmgp-1(tm5483)]
MYM 002 [nmgp-1(gk144571)]
*
% alive worms
100
75
50
25
0
0
5
10
15
20
time (days)

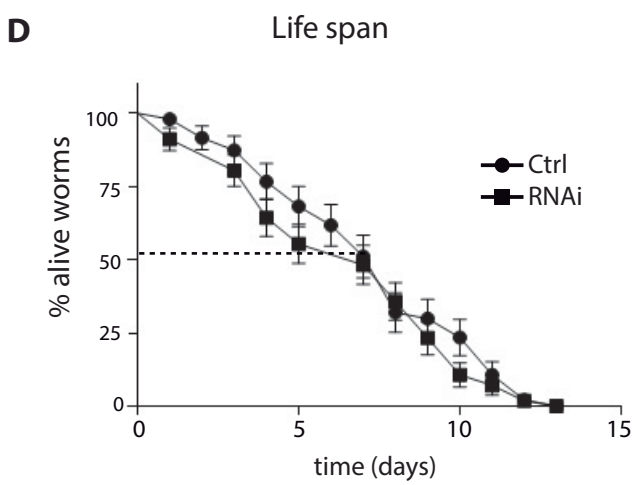
D
Life span
Ctrl
RNAi
% alive worms
100
75
50
25
0
0
5
10
15
time (days)

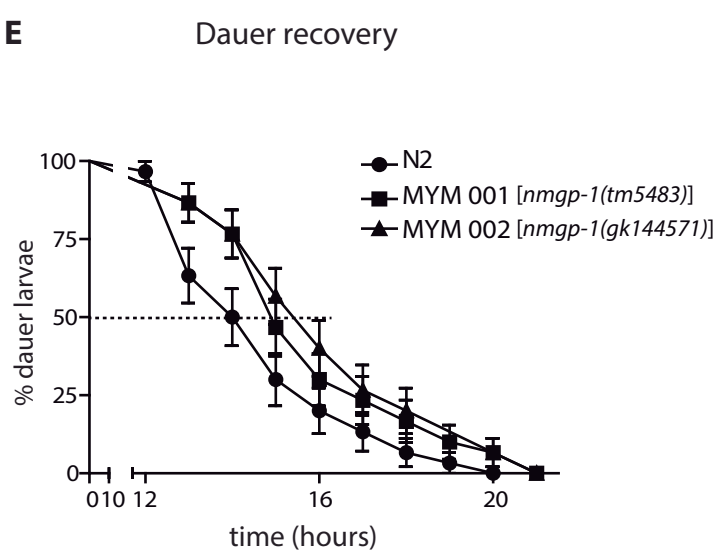
E
Dauer recovery
N2
MYM 001 [nmgp-1(tm5483)]
MYM 002 [nmgp-1(gk144571)]
% dauer larvae
100
75
50
25
0
0
10
12
16
20
time (hours)

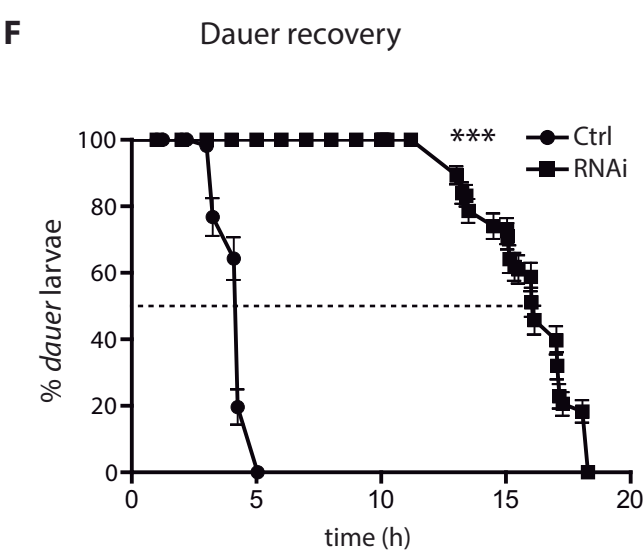
F
Dauer recovery
***
Ctrl
RNAi
% dauer larvae
100
80
60
40
20
0
0
5
10
15
20
time (h)

Figure 6

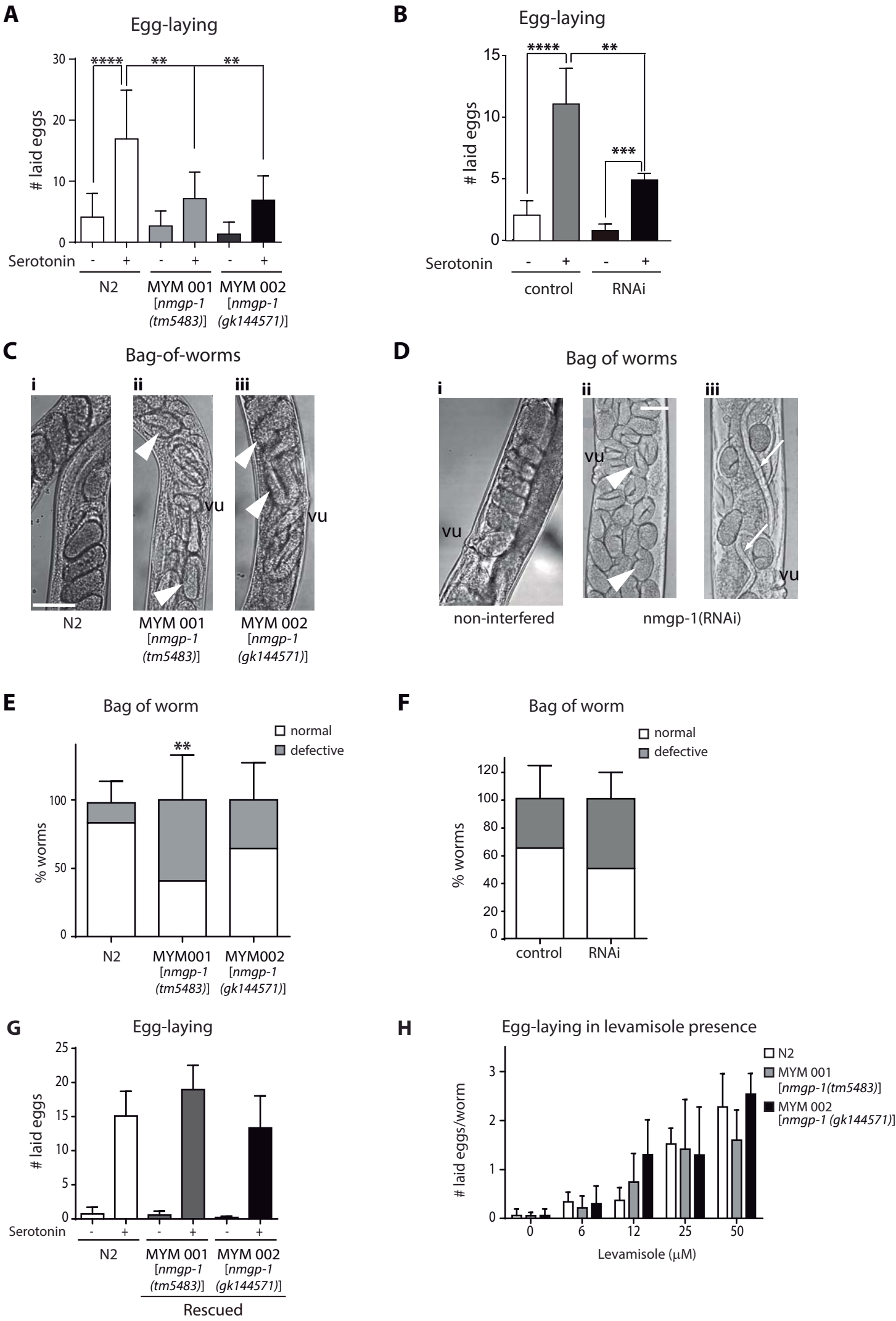
A
Egg-laying
laid eggs
Serotonin
N2
MYM 001 [nmgp-1 (tm5483)]
MYM 002 [nmgp-1 (gk144571)]
B
Egg-laying
laid eggs
Serotonin
control
RNAi
C
Bag-of-worms
i
ii
iii
vu
N2
MYM 001 [nmgp-1 (tm5483)]
MYM 002 [nmgp-1 (gk144571)]
D
Bag of worms
i
ii
iii
vu
non-interfered
nmgp-1(RNAi)
E
Bag of worm
normal
defective
% worms
N2
MYM001 [nmgp-1 (tm5483)]
MYM002 [nmgp-1 (gk144571)]
F
Bag of worm
normal
defective
% worms
control
RNAi
G
Egg-laying
laid eggs
Serotonin
N2
MYM 001 [nmgp-1 (tm5483)]
MYM 002 [nmgp-1 (gk144571)]
Rescued
H
Egg-laying in levamisole presence
laid eggs/worm
N2
MYM 001 [nmgp-1(tm5483)]
MYM 002 [nmgp-1 (gk144571)]
Levamisole (µM)

Figure 7

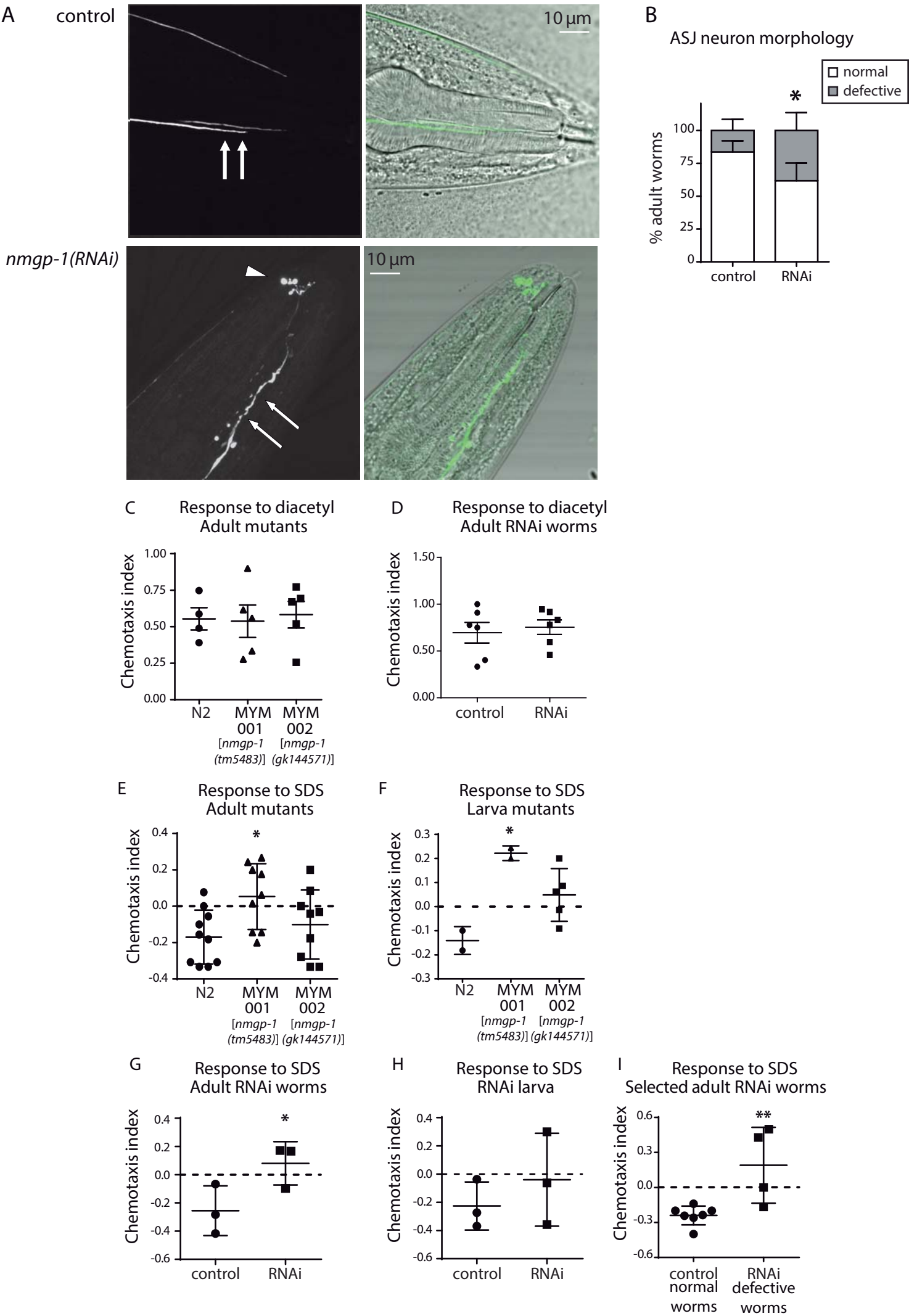
A
control
10 µm
nmgp-1(RNAi)
10 µm
B
ASJ neuron morphology
normal
defective
% adult worms
100
75
50
25
0
*
control
RNAi
C
Response to diacetyl
Adult mutants
Chemotaxis index
1.00
0.75
0.50
0.25
0.00
N2
MYM 001 [nmgp-1 (tm5483)]
MYM 002 [nmgp-1 (gk144571)]
D
Response to diacetyl
Adult RNAi worms
Chemotaxis index
1.50
1.00
0.50
0.00
control
RNAi
E
Response to SDS
Adult mutants
Chemotaxis index
0.4
0.2
0.0
-0.2
-0.4
*
N2
MYM 001 [nmgp-1 (tm5483)]
MYM 002 [nmgp-1 (gk144571)]
F
Response to SDS
Larva mutants
Chemotaxis index
0.3
0.2
0.1
0.0
-0.1
-0.2
-0.3
*
N2
MYM 001 [nmgp-1 (tm5483)]
MYM 002 [nmgp-1 (gk144571)]
G
Response to SDS
Adult RNAi worms
Chemotaxis index
0.4
0.2
0.0
-0.2
-0.4
-0.6
*
control
RNAi
H
Response to SDS
RNAi larva
Chemotaxis index
0.4
0.2
0.0
-0.2
-0.4
-0.6
control
RNAi
I
Response to SDS
Selected adult RNAi worms
Chemotaxis index
0.6
0.3
0.0
-0.3
-0.6
**
control normal worms
RNAi defective worms